

EVALUATING FACTORS THAT CONTROL RECHARGE IN A THICK VADOSE
ZONE UNDER CLIMATE VARIABILITY AND CHANGE

A thesis submitted to the faculty of
San Francisco State University
In partial fulfillment of
the requirements for
the Degree

Master of Science

In

Geosciences

by

Cassandra Wolf

San Francisco, California

May 2020

Copyright by
Cassandra Wolf
2020

CERTIFICATION OF APPROVAL

I certify that I have read Evaluating Factors that Control Recharge in a Thick Vadose Zone Under Climate Variability and Change by Cassandra Wolf, and that in my opinion this work meets the criteria for approving a thesis submitted in partial fulfillment of the requirement for the degree Master of Science in Geoscience at San Francisco State University.



Jason J. Gurdak, Ph.D.
Associate Professor



Leora Nanus, Ph.D.
Assistant Professor



Alexander (Zan) Stine, Ph.D.
Associate Professor

EVALUATING FACTORS THAT CONTROL RECHARGE IN A THICK VADOSE ZONE UNDER CLIMATE VARIABILITY AND CHANGE

Cassandra Wolf
San Francisco, California
May 2020

Groundwater is an important freshwater resource, especially in areas that rely almost completely on groundwater and where overdraft conditions can occur. Climate variability and change pose uncertainties in the sustainability of groundwater resources. Understanding how factors including land use/land cover (LULC), climate conditions (precipitation, air temperature), and recharge mechanisms (diffuse and irrigation recharge) respond to climate variability and change can help improve the inflow component of future groundwater budgets and inform groundwater sustainability planning and related policy decisions. In this study, I used Hydrus-1D to model vadose zone flux for six sites in the Central Platte Natural Resources District (CPNRD) of central Nebraska. The six sites represent spatial and temporal climate variations and the dominant recharge mechanisms (diffuse and irrigation) under LULC of the study area. Historical recharge and total potential profiles were simulated in Hydrus-1D for the years 1950-2018 and future recharge and total potential profiles were simulated in Hydrus-1D for the years 1950-2100 using an ensemble of nine downscaled global climate models (GCMs) at representative concentration pathways (RCPs) 4.5 and 8.5. Future recharge showed more recharge under irrigated sites compared to rangeland sites in their respective locations (west and east). Future recharge was also projected to decrease over time, with larger decreases under RCP 8.5. Historical recharge was compared to historical periods of increased precipitation and drought and a Palmer Drought Severity Index (PDSI) timeseries adjusted for lag correlations. Findings showed recharge correlated with PDSI and LULC controlled the recharge response time; corn crop sites within 20-24 months where rangeland sites responded within 58-372 months. Total potential profiles were calculated using head at depth outputs from Hydrus-1D. Historic total potential profiles for each site representing dates surrounding the most recent wet and dry period showed spatial variations in precipitation to be a controlling factor of total potential responses to climate variability. Western sites that receive less average annual precipitation showed less downward flux during dry periods and more downward flux during wet periods, whereas eastern sites that receive more average annual precipitation showed less downward flux during wet periods compared to dry periods but more upward seasonal flux during dry periods. Future total potential profiles were calculated using one of the GCMs at both RCPs 4.5 and 8.5 for the years 2040 and 2099 where findings showed more seasonal upward flux at all sites in the year 2099 under RCP 8.5.

I certify that the abstract is a correct representation of the content of this thesis.



Chair, Thesis Committee



Date

ACKNOWLEDGEMENTS

This research was funded by a grant from the Water Sustainability Fund of the Nebraska Natural Resources Commission in collaboration with the Central Platte Natural Resources District (CPNRD) and the U.S. Geological Survey (USGS) Nebraska Water Science Center. In particular, I want to thank Duane Woodward (CPNRD) and Chris Hobza (USGS) for helping with the installation, maintenance, and data sharing from the vadose zone monitoring network. I also thank Dr. Ed Maurer (Santa Clara University) for providing guidance and compiling the downscaled Localized Constructed Analogs (LOCA) data from the ensemble of global climate models (GCMs) that I used to drive my Hydrus-1D models. I also acknowledge the World Climate Research Programme's Working Group on Coupled Modelling, which is responsible for CMIP, and thank the climate modeling groups (listed in Table 3 of this thesis) for producing and making available their model output. For CMIP the U.S. Department of Energy's Program for Climate Model Diagnosis and Intercomparison provides coordinating support and led development of software infrastructure in partnership with the Global Organization for Earth System Science Portals. I want to thank David Dawdy for the Dawdy Hydrologic Research Award.

I want to extend my deepest appreciation for my committee chair, Dr. Jason Gurdak. His guidance and expertise have made this an invaluable learning experience. I also want to thank my committee members, Dr. Zan Stine and Dr. Leora Nanus, for their gracious support and assistance in my project. I am also very grateful for my fellow graduate students for their friendship and support; it has been such a pleasure to learn from them and share in this experience together.

Lastly, I want to share my deepest gratitude for my friends and family that have loved and supported me through this experience. And, a special thank you to my mom, Cathy; I love you.

TABLE OF CONTENTS

List Of Tablesix

List Of Figures x

Introduction..... 1

Research Goals 4

Background..... 4

Methods 6

 Site Selection 7

 Model Parameters 7

 Observation Sites 8

 Land Use And Land Cover 9

 Historical Simulations..... 10

 Model Assumptions 11

 Spin-Up Method 11

 Calibration 12

 Simulations Of Future Recharge Under Climate Change 14

 Response Of Historical Recharge To Climate Variability..... 17

 Statistical Analyses 18

Results And Discussion 18

 Precipitation Trends..... 19

 Evapotranspiration Trends..... 20

 Irrigation Requirement Trends..... 21

 Future Recharge Trends..... 22

 Historic Recharge Trends With Climate Variability 24

 Historic Total Potential Profiles 26

 Future Total Potential Profiles 28

Conclusion 30

Tables..... 33

Figures	38
References.....	50

LIST OF TABLES

Table	Page
1. Vadose zone monitoring well sites in the CPNRD.....	33
2. NSE values of observed versus simulated monthly total potential profile slopes for calibration.....	34
3. Downscaled global climate models (GCMs) used in this study.....	35
4. Lag correlations of simulated historic recharge and PDSI values.....	36
5. Historic wet and dry periods PDSI and recharge values.....	37

LIST OF FIGURES

Figures	Page
1. Observed monitoring-well seasonal variability and persistent upward gradient of total potential.....	38
2. Land use map of CPNRD.....	39
3. Location of study sites in the High Plains with temperature and precipitation gradients.....	40
4. Simulated precipitation from 1950-2100 for RCP 4.5 and RCP 8.5 at each site based on LOCA downscaled output from GCMs.....	41
5. Simulated evapotranspiration calculated in Hydrus-1D from 1950-2100 for RCP 4.5 and RCP 8.5 at each site based on LOCA downscaled output from GCMs....	42
6. Simulated irrigation requirements for irrigated sites calculated in Hydrus-1D from 1950-2100 for RCP 4.5 and RCP 8.5 at each site based on LOCA downscaled output from GCMs.....	43
7. Simulated recharge calculated in Hydrus-1D from 1950-2100 for RCP 4.5 and RCP 8.5 at each site based on LOCA downscaled output from GCMs.....	44
8. Simulated historic recharge from Hydrus-1D compared to PDSI values from 1950-2018 at each site.....	45
9. Simulated historic recharge from Hydrus-1D adjusted with lag correlations and compared to PDSI values from 1950-2018 at each site.....	46
10. Recent historical total potential profiles calculated from head at depth outputs from Hydrus-1D for recent wet/dry periods for each site.....	47

11. Simulated future total potential profiles of GCMs at RCP 4.5 calculated from head at depth outputs from Hydrus-1D.....	48
12. Simulated future total potential profiles of GCMs at RCP 8.5 calculated from head at depth outputs from Hydrus-1D.....	49

INTRODUCTION

Climate change poses uncertainties regarding the sustainability of freshwater, including groundwater resources (Green et al., 2011). At the global scale, groundwater supports more than 40% of all personal, industrial, and agricultural uses, but some regions and communities, particularly in semi-arid and arid climates, can be closer to 100% reliant on groundwater (Taylor et al., 2012). Recently, groundwater sustainability has become a priority for many regions because of widespread aquifer depletion, which occurs when rates of groundwater use and other outflows exceed the rates of recharge and other inflows. An aquifer is in overdraft conditions if outflows consistently exceed inflows; an aquifer cannot be a sustainable resource if overdraft conditions persist.

Overdraft conditions can occur during drought and because of population growth and the associated increased demand for food, water, and energy (Treidel et al., 2012). It is likely that climate change will produce more extreme periods of precipitation and drought; these changes in temperature and precipitation associated with climate change will likely affect recharge mechanisms and rates to aquifers (Green et al., 2011; Meixner et al., 2016; Taylor et al., 2012). The Intergovernmental Panel on Climate Change (IPCC) project higher average air temperatures and alterations in the magnitude and frequency of precipitation over the 21st century (Green et al., 2011). Recharge is one of the most important but challenging water budget components to quantify, particularly under projected future climate change. A better understanding of the factors that affect recharge

rates and mechanisms can improve the inflow component of future groundwater budgets and inform groundwater sustainability planning and related policy decisions.

Factors that affect natural recharge include land use/land cover (abbreviated as LULC), climate conditions (precipitation, air temperature, relative humidity, etc.), and recharge mechanisms (diffuse and irrigation recharge). Diffuse recharge is water from precipitation, including rain and snow, and irrigation recharge is irrigation return flow that infiltrates the land surface and flows through the vadose zone to reach the water table. Mountain block recharge is another important recharge mechanism for some basins but is not a focus of my research. Similarly, managed recharge, which includes the purposeful diversion of surface water into percolation ponds and losing streams, is also important for sustainable groundwater management, but is not a focus of this research. Local, site-specific understanding of climate and subsurface geology is necessary when estimating recharge due to spatial and temporal variability (McMahon et al., 2011). Interannual to multidecadal climate variability has also been shown to be an important control on recharge rates in many aquifer systems of the U.S. (Kuss and Gurdak, 2014), including the High Plains aquifer, which is the focus of this research.

Diffuse recharge occurs beneath natural LULC and can be sensitive to changes in precipitation and air temperature (Meixner et al., 2016), which affects evapotranspiration (ET), soil water content, and most importantly the total potential gradients in the vadose zone that drives water movement and recharge (Gurdak et al., 2007.) The vadose zone is the unsaturated (or variably saturated) portion of an aquifer above the water table. Here,

we refer to recharge as water that has intercepted the water table after infiltrating through the soil and a downward flux through the vadose zone. Recharge can also occur from subsurface flow between hydrogeologic units, which we do not consider here.

In the vadose zone, water flows from areas of higher total potential to lower total potential. In some regions, particularly semi-arid and arid climates, capillary and adsorptive forces of the soil matrix on water can cause either seasonal or persistent upward flow due to an upward total potential gradient towards land surface. Seasonal upward total potential gradients can occur during the summer or fall when ET rates increase (Wellings and Bell, 1982) (Figure 1a). Persistent upward total potential gradients have been observed in some arid climate (Figure 1b) and have developed over the geologic timescales (Gurdak et al., 2007; McMahon et al., 2006; Walvoord et al., 2004). Whether seasonal or persistent, upward total potential gradients can limit or prevent the downward flux of water through the vadose zone, which ultimately limits or prevents recharges. LULC and associated ET rates can influence the dynamics of total potential gradients, and thus are a potentially important controlling factor for recharge to an underlying aquifer. Depth of rooting of vegetation, wilting point, and fractional vegetation coverage are vegetation parameters that can alter ET rates and soil moisture, and thus total-potential gradient dynamics, and in turn, the timing and rates of recharge (Scanlon et al., 2005). To-date, few studies on the response of recharge to climate change have explored the underlying processes and mechanisms in thick vadose zones (Meixner et al., 2016). Moreover, no studies have explored how total

potential gradients may respond to future climate change. In this study, I explore these underlying processes and mechanisms and their response to climate change and variability.

RESEARCH GOALS

To address the previously described knowledge gaps, the overarching purpose of my thesis is to evaluate how the spatial and temporal patterns of natural recharge rates and mechanisms (diffuse and irrigation recharge) in thick vadose zones, ranging from 14.2 m to 38.9 m, respond to a range of factors, including LULC and climate variability and change over the 21st century. I will do this using a suite of long-term data from the vadose zone to calibrate Hydrus-1D (Šimůnek et al., 2008) models and run a series of scenarios to simulate historic and future projected recharge and systematically test the above-mentioned factors. The models and scenarios will focus on the Central Platte watershed in the northern High Plains aquifer of Nebraska where an extensive dataset from the vadose zone is being collected (Gurdak et al., 2007; Lauffenburger et al., 2018; Steele et al., 2014). The High Plains aquifer is widely recognized as groundwater resources that is facing serious sustainability challenges (Konikow, 2013; Treidel et al., 2012).

BACKGROUND

Few studies have used field data from thick vadose zones to calibrate and validate numerical models of climate variability and change effects on recharge in semi-arid and arid aquifers systems, such as the High Plains aquifer (Crosbie et al., 2013; Lauffenburger

et al., 2018; Scanlon et al., 2003). A previous study by Lauffenburger et al. (2018) in the northern High Plains aquifer used different vadose zone sites and ensemble of GCMs with Hydrus-1D to model two global warming scenarios, low warming (+1.0 °C) and high warming (+2.4 °C) for the year 2050. Projections of precipitation, irrigation, ET, and diffuse and irrigation recharge rates for both warming scenarios at 2050 were compared to a baseline of 1990. The results showed no statistical difference in the low warming scenario of 2050 compared to 1990 but showed increased ET and irrigation requirements and decreased recharge in the high warming scenario of 2050 compared to 1990. Statistical differences were also shown between the western and eastern sites and between rangeland and irrigated sites for both warming scenarios and the historic baseline (Lauffenburger et al., 2018). However, the Lauffenburger et al. (2018) study did not evaluate the total potential gradients in the vadose zone.

My study area is within the Central Platte Natural Resources District (CPNRD), which is located in central Nebraska overlying the northern High Plains aquifer (Figure 2). The High Plains aquifer is one of the most stressed in the U.S. and has large depletions in groundwater storage (Konikow, 2013). The region is arid to semi-arid with moderate precipitation and high evaporation (Gurdak et al., 2007). The High Plains aquifer system is the largest groundwater resource in the central U.S. supplying a large percentage of the country's grains (corn, wheat, and sorghum), but relies nearly 100% on groundwater pumping to support the irrigated agriculture (Gurdak et al., 2009). As result of this dependency it had the highest depletion rate of U.S. aquifer systems in the 20th century

(Konikow, 2015). Previous High Plains groundwater models of future recharge show spatial patterns; there is a north-south gradient of recharge with decreases in the south to moderate increases in the north due to spatial climate gradients (Konikow, 2015; Meixner et al., 2016). Diffuse recharge is the primary mechanism in the northern High Plains aquifer, accounting for an estimated 85% of the total recharge (Meixner et al., 2016).

METHODS

To evaluate factors that control the spatial and temporal patterns of natural recharge in thick vadose zones, such as LULC and historic and projected climate variability and change, I built Hydrus-1D (Šimůnek et al., 2008) models that represent monitoring sites in the CPNRD and used them to simulate total potential gradients, water flux through the vadose zone, and recharge rates. Hydrus-1D is a numerical modeling software package that solves the Richards' equation, below (Richards, 1931) for flow in one-dimensional variably saturated porous media (Šimůnek et al., 2013).

$$\frac{\partial \theta}{\partial t} = \frac{\partial}{\partial x} \left[K \left(\frac{\partial h}{\partial x} + \cos \alpha \right) \right] - S \quad \text{Equation 1}$$

Where h is the water pressure head, θ is the volumetric water content, t is time, x is the spatial coordinate, S is the sink term, α is the angle between the flow direction and the vertical axis, and K is the unsaturated hydraulic conductivity function (Šimůnek et al., 2013).

Simulated head values from the vadose zone and recharge rates from each model were analyzed to evaluate the controlling factors of recharge.

Site Selection

A Hydrus-1D model was created for each of six CPNRD sites; four of these models were created by Zach Lauffenburger and reported in Lauffenburger et al., (2018) and I created the remaining two models. The sites and corresponding models are described and named as follows: western rangeland (WR), western irrigated corn (WIC), eastern rangeland (ER), eastern rangeland 2 (ER2), eastern irrigated corn (EIC), and eastern dryland corn (EDC) (Table 1). These six sites were selected because they represent diffuse and irrigated recharge settings in the most dominant LULC of the northern High Plains aquifer (Steele et al., 2014) (Figure 2) as well as the west to east gradient in average annual precipitation (Figure 3).

Model Parameters

All six Hydrus-1D models use the van Genuchten-Mualem single porosity model with no hysteresis to represent the soil-moisture retention function (Šimůnek et al., 2013). The upper boundary of the models was defined as an atmospheric boundary condition with surface run off and the lower boundary was considered the bottom of the vadose zone and freely draining. Therefore, the simulated flux from the bottom of the model domain represents recharge to the water table.

The hydraulic parameters of the models are based on data collected from each of the six vadose zone monitoring sites within the CPNRD (Figure 2). The site locations were chosen to be representative of the east-west gradient in mean annual precipitation and the most common natural and agricultural LULC types in the northern High Plains aquifer (Figure 2). Historical annual data shows greater precipitation at the Grand Island meteorological station (eastern study area) than the Gothenburg meteorological station (western study area) (NOAA, 2018).

Observation Sites

Installation of the study sites took place between 2008 and 2010 and followed methods described in Gurdak et al., (2007) and McMahon et al., (2006, 2003). At each site, a 15 cm hollow-stem auger was used to drill a borehole down to the water table. During drilling, continuous soil-core samples from the vadose zone were collected using split-spoon core barrel methods as described by Steele et al. (2014). Soil texture information from the soil-core samples, including percent sand, silt, and clay and bulk density, were input into Hydrus-1D using the Rosetta Dynamically Linked Library to calculate water retention parameters and saturated hydraulic conductivity; those parameters were used to build the vadose zone strata columns for each model (Schaap et al., 2001; Šimůnek et al., 2008).

At each site, a series of heat dissipation probes (HDPs) were installed within the boreholes at various depths, as described in Gurdak et al. (2007) and McMahon et al.

(2003). The HDPs are used to measure in-situ matric potential (KPa) on 15-minute intervals (Campbell Scientific Inc., 2009; Steele et al., 2014). The total potential at each HDP depth within the vadose zone is calculated as the sum of the observed matric potential values and the gravitational potential (m), using land surface as the datum. Osmotic potential is assumed negligible for these total potential calculations (McMahon et al., 2006). The calculated total potential time series were used during calibration of the Hydrus-1D models and validation of the simulated total potential gradients.

Land Use and Land Cover

Root water uptake was simulated for each Hydrus-1D model with parameters defined by Feddes et al., (1978) and specific values for corn and rangeland from Wesseling et al., (1991). The rangeland sites (ER, ER2, and WR) simulate ground cover of mixed-grass prairie plant species with a crop height of 2 m and rooting depth of 2.5 m (Lauffenburger et al., 2018). The corn sites (EIC, EDC, and WIC) simulate ground cover of seasonal corn crops, from late June to mid-September, with a maximum root height of 2 m and rooting depth of 1.7 m (Lauffenburger et al., 2018). Irrigation requirements were calculated for sites EIC and WIC. The models of the irrigated sites were first run with input from each GCM, which are described in the following sections. The Hydrus-1D model outputs of ET*, evaporation, transpiration, net shortwave radiation*, net longwave radiation*, radiation term*, aerodynamic term*, precipitation, interception, and excess interception (*terms calculated from the Penman-Monteith combination equation) (Šimůnek et al., 2013) from each run were input into the Nebraska Department of Natural

Resources Crops Simulation Model (CROPSIM) as outlined in Lauffenburger et al., (2018) CROPSIM uses these inputs to calculate irrigation requirements for corn crops during peak irrigation seasons from late June to mid-September of each year of the run. The calculated irrigation requirements were then added to precipitation inputs and the models were run again; outputs from the second run were then used for analysis for both irrigated sites.

Historical simulations

Historical climate data sets were collected from the National Oceanic and Atmospheric Administration (NOAA) National Climatic Data Center (NCDC) (NOAA, 2018) to provide daily timeseries inputs of minimum and maximum air temperature and precipitation for the Hydrus-1D models to simulate recharge and total potential profiles for historic purposes. Eastern and western sites used NOAA historical data sets from Grand Island (sites: ER, ER2, EIC, and EDC) and Gothenburg (sites: WR and WIC) meteorological stations, respectively, based on their proximity to the sites. Simulated minimum and maximum air temperature and precipitation from a suite of GCMs were used as inputs in the models to simulate historic and future recharge. Evapotranspiration (ET) was calculated by Hydrus-1D using the minimum and maximum air temperature as inputs in the Penman-Monteith combination equation (Šimůnek et al., 2013) Additional climate inputs of relative humidity (RH), wind speed, and radiation were collected from historical

data from Lauffenburger et al. (2018), averaged for each day of the year, and repeated for every year of the run and used for every model.

Model Assumptions

The Hydrus-1D models are numerical representations of six observation well study sites located in the CPNRD, and a few assumptions were made to simplify the natural complexity of the interactions between the atmosphere, vadose zone, and water table. The first assumption made in the models is that the thickness of the vadose zone does not change with time; depth to the water table at the time of well installation for each site was used as the vadose zone thicknesses ranging from 14.2 m to 38.9 m. This implies that the water table depth remains the same over time since I am considering any water leaving the bottom of the vadose zone model as recharge. The next assumption in the model is that daily relative humidity, wind speed, and radiation repeat each year; this is explained in the previous section (Historical Simulations). Another assumption for the models is that each sites LULC does not change over time. Realistically, agricultural expansion occurs frequently where rangeland is converted to cropland (Scanlon et al., 2005).

Spin-up Method

Historical climate data from 1950 to 1980 were used in model spin-up simulations for each site. Running spin-up models is common practice in hydrologic modeling, especially for integrated models that simulate interactions between the atmosphere, surface

water, and groundwater (Ajami et al., 2014; Seck et al., 2015). The purpose of a spin-up model is to address uncertainties in initial condition inputs inherent in modelling by running the model for a duration of time to achieve an equilibrium, either steady-state or dynamic, in soil moisture content and temperature (Ajami et al., 2014; Seck et al., 2015). Once equilibrium is reached, soil moisture outputs are then used as the initial condition inputs in the model intended for the study to effectively simulate integrated hydrologic systems (Seck et al., 2015). For this study, preliminary spin-ups were run for each site's model using historical NOAA climate data from 1950-1980 to achieve equilibrium in soil moisture contents of the vadose zone profile. Spin-up outputs of the soil moisture profile were then used as the initial water content conditions of the subsequent model runs.

Calibration

To calibrate the Hydrus 1-D models, I used a manual trial and error approach for history matching, which included qualitative and quantitative methods to compare simulated and observed total potential values from the HDPs that were collected between 2008 and 2017. The qualitative method involved visually comparing the simulated and observed total potential profiles. In general, the calibrated models provide reasonable simulation of the seasonal dynamics in the total potential profiles observed at the six sites. The quantitative method relied on the Nash-Sutcliffe coefficient of efficiency (NSE), which is a common statistic used in the calibration of hydrologic models. The NSE is normally calculated using observed and simulated total potential, but because of the variation in climate and land use input data into the models, I calculated the NSE using

observed and simulated total potential slopes below the rooting zone. I calculated the NSE as:

$$NSE = \frac{\sum_{i=1}^n |(X_{t,m} - X_{t,s})|_i^2}{\sum_{i=1}^n |(X_{t,m} - \bar{X}_{t,m})|_i^2} \quad \text{Equation 2}$$

where $X_{t,m}$ is the measured (observed) total potential slope, $X_{t,s}$ is the simulated total potential slope, and $\bar{X}_{t,m}$ is the mean of the measured total potential slope. NSE values range from $-\infty$ to 1, where values close to 1 indicate a good fit (Anderson et al., 2015). For NSE values of 0, the mean of the data is as good a predictor as the simulated values; and for a value less than 0, the mean of the data would be a better predictor (Anderson et al., 2015). The calculated NSE values were generally close to 1, ranging from -2.76 to -0.03 (Table 2) and indicate a reasonably good fit between the simulated and observed total potential values.

Historical NOAA climate data from 2008 to 2017 were used as meteorological and atmospheric model inputs because it is during this time period that instrumentation at the sites have been collecting data. The Hydrus-1D models were built with simulated observation nodes in the model profile at the same depths as the HDPs in the vadose zone of each site. Timeseries outputs of head, in meters, are simulated for each observation node for the duration of the model run. Total potential timeseries for each model observation node was calculated by summing the head values and the gravitational potential at each observation node. Generally, total potential is calculated by summing matric potential and the gravitational potential, which is the elevation of the observation point above a chosen

reference datum; for the Hydrus-1D observation nodes, head outputs are used as the matrix potential values (Radcliffe, D.E., 2010; Wellings and Bell, 1982). Ground level was chosen as the reference datum, which causes the gravitational potential values to be negative. The Hydrus-1D observation node and calculated HDP total potential data were given in inconsistent timesteps, so all total potential timeseries were processed to achieve average daily and monthly timeseries for calibration purposes. Monthly total potential profile of the vadose zone calculated from model outputs and observed field data; the slopes of the profiles below the rooting zone were visually compared to calibrate each model. Generally, the total potential slopes from the observed data varied more than the modeled total potential slopes but overall looked similar.

Simulations of Future Recharge under Climate Change

To simulate future recharge, I used projected future changes in precipitation and temperature for the sites using downscaled climate model data for the years 1950-2100. Future projections were based on output from global climate model (GCM) simulations conducted as part of the Coupled Model Intercomparison Project - Phase 5 (K. E. Taylor et al., 2012). The CMIP5 experiments formed the basis for the climate model simulations included in the 5th assessment of the Intergovernmental Panel on Climate Change (Stocker, 2014) (IPCC, 2013). The GCMs used in this study are listed in Table 3. These GCMs were selected based on 1) the availability of complete daily precipitation and temperature data for both a historical period and future projections, 2) available output for both a higher business-as-usual emissions pathway (representative concentration pathways (RCP) 8.5)

and a lower emissions pathway (RCP 4.5). Furthermore, eight of these nine GCMs were included in a previous study (Polade et al., 2013) that demonstrated successful simulation of important teleconnections between oceanic oscillations (such as ENSO and PDO) and North American precipitation, important features for this study. An ensemble of nine GCMs is large enough where characterization of ensemble mean and variability tends to be relatively insensitive to the individual selection of GCMs (Maurer et al., 2014).

For each GCM, I used RCPs of $+4.5 \text{ W/m}^2$ and $+8.5 \text{ W/m}^2$, each will be referred to as RCP 4.5 and RCP 8.5, respectively. RCP 4.5 is a global climate projection scenario where total global radiative forcing stabilizes by 2040 due to policies, strategies, and technologies expected to be enacted to reduce greenhouse gas emissions (Clarke et al., 2007; Smith et al., 2006; Wise et al., 2009). RCP 8.5 is a scenario where greenhouse gas emissions continue to increase at the same rate as is happening currently without any strategies employed to decrease emissions ("RCP Database (version 2.0)," 2009; Riahi et al., 2007).

The GCM output was statistically downscaled to a fine degree spatial resolution producing daily precipitation and temperature (maximum and minimum) using the recently-developed localized constructed analogs (LOCA) (Pierce et al., 2014). The LOCA method was developed to maintain specific hydrologically important characteristics including spatial correlations of events and low frequency variability, and has been incorporated in a publicly available dataset of downscaled data (Bracken, 2016). The LOCA method uses an analog matching algorithm to downscale large-scale GCM output

to fine scales, ensuring that the daily downscaled fields of precipitation and, minimum/maximum temperature are consistent on both regional and local spatial scales. LOCA begins by correcting the annual cycle so that both the GCM and observations display the same seasonality in both temperature and precipitation. Using a seasonal window, the distributions of precipitation and temperature are corrected using methods similar to quantile mapping (Li et al., 2010) for temperature and the PresRat (Pierce et al., 2015) method for precipitation. A frequency-dependent bias correction (Pierce et al., 2015) is then applied to the time series, adjusting the amplitude of GCM variability in frequency bands from two days to 11 years to better match the observations. Finally, the downscaling procedure begins by establishing coarse resolution analog points with a defined surrounding region with positively correlated meteorology. An analog day is selected from the historical record, and the final downscaled field is constructed by scaling the fine scaled observations, at $1/16^\circ$ for this application, for that day to match bias corrected GCM meteorology.

Each Hydrus-1D model was run with LOCA downscaled precipitation and minimum and maximum air temperature output from each GCM. Therefore, the total ensemble of Hydrus-1D output for each of the six sites includes 18 model scenarios (nine GCMs each at RCP 4.5 and 8.5). The primary Hydrus-1D output analyzed here was the daily simulated bottom flux (recharge) from each of the nine GCM model scenarios each at RCP 4.5 and 8.5 for the years 1950 to 2100 and head at depth from the CANESM2 GCM at RCP 4.5 and 8.5 used to calculate simulated future total potential profiles for the years

2040 and 2099. I selected the CANESM2 to simulate the total potential profiles because this GCM is approximately average in terms of forecast precipitation and temperature from the nine GCMs (Table 3).

Response of Historical Recharge to Climate Variability

To evaluate the effects of climate variability on recharge, I modeled historical recharge and total potential profiles in the vadose zone for each of the six sites and compared the outputs to historical periods of above average precipitation and drought, which I refer to as wet and dry periods. Historical precipitation and minimum and maximum air temperature data for the years 1950-2018 were gathered from (NOAA, 2018) for Gothenburg, NE and Grand Island, NE to represent the western and eastern sites respectively. Based on the monthly Palmer Drought Severity Index (PDSI) (NOAA, 2018), I chose five each of the most recent and prominent wet and dry periods for central Nebraska. Dry periods are indicated by negative PDSI values and wet periods are indicated by positive PDSI values. A timeseries of simulated recent historic recharge rates for each site was visually compared and statistically correlated to a timeseries of PDSI values as well as a phase lag time correlation of historic recharge timeseries to PDSI values using HydroClimATe: Hydraulic and Climatic Analysis Toolkit (Dickinson et al., 2014). HydroClimATe was used to calculate time lag correlations of historic recharge timeseries to PDSI values for each site for time lags of 1-414 months. The monthly phase lag with the highest correlation coefficient for each site was determined and used to compare a phase-adjusted timeseries of historic recharge to PDSI values. Daily snapshots of total potential

profiles were created for the most recent wet and dry periods to evaluate the effects of climate variability on total potential profiles.

Statistical Analyses

I used the Kruskal-Wallis non-parametric test with an alpha level (α) of 0.05 to determine differences between the non-parametric groups of data (Helsel and Hirsch, 1992). Subsequently, I used the Steel-Dwass All Pairs test, which is equivalent to the non-parametric version of the Tukey test to determine differences among the groups of data (JMP, 2009). I used these statistical tests to analyze the differences between (i) historical and future simulated values, (ii) the six sites, and (iii) RCP 4.5 and 8.5.

RESULTS AND DISCUSSION

The results of the simulated historical (1950-2009) and future (2010-2100) precipitation, ET, irrigation requirements, and recharge at each of the six sites using the 18 GCM model scenarios are shown in Figures 4-7, respectively. To evaluate future changes in recharge over the 21st century, the results in Figures 4-7 are presented for the following future time periods: 2010-2039, 2040-2069, and 2070-2099. The effects of the west-east gradient in average annual precipitation (western (W) and eastern (E)) and LULC (rangeland (R), irrigated cornland (IC), and dryland corn (DC)) are also shown in Figures 4-7, as well as in Figure 8-9 that shows recharge response to historical climate variability and Figures 10-12 that shows historic and future total potential profile dynamics. The results are discussed next.

Precipitation Trends

Precipitation outputs from the nine GCMs and RCP 4.5 and 8.5 ranged from 183 to 1,528 mm/year across all sites (Figure 4). Under both RCP 4.5 and 8.5, most of the six sites appear to have a temporal increase in the median precipitation from the historical (1950-2009) to late 21st century (2070-2099) (Figure 4). The visual observations of an increase in median precipitation over the 21st century was confirmed using the Steele-Dwass test (α -level = 0.05).

Under RCP 4.5, comparisons of time periods for each site showed precipitation for historic (1950-2009), early-21st century (2010-2039), mid-21st century (2040-2069), and late-21st century (2070-2099) were not statistically different at sites WR, ER, ER2, EIC, and EDC. Site WIC indicated statistical differences in precipitation between late-21st (2070-2099) and both historic (1950-2009) (p-value=0.0106) and early-21st century (2010-2039) (p-value=0.0017).

Comparisons of precipitation in each of the time periods under RCP 4.5, precipitation for all sites for the historic (1950-2009) and early-21st century (2010-2039) are not statistically different (p-value=0.184) and similarly, the mid- (2040-2069) and late-21st century (2070-2099) are not statistically different (p-value = 0.919). These results indicate a statistical difference in median precipitation between early- and mid-21st century, but the median precipitation remains relatively constant between the mid- and late-21st century. These findings are consistent with the RCP 4.5 scenario where radiative forces stabilize by 2040.

Under RCP 8.5, comparisons of time periods for each site showed precipitation was not statistically different over time at the non-irrigated sites (WR, ER, ER2, and EDC). Sites WIC and EIC indicated statistical differences between precipitation in the late-21st (2070-2099) and historic (1950-2009) (p-value=0.0069 and 0.001 respectively).

Under RCP 8.5, precipitation for the late-21st century (2070-2099) was statistically different than precipitation for both historic (1950-2009) and early-21st century (2010-2039) time periods (p-value= 0.0001 and 0.0243 respectively) for all sites. Elevated projected precipitation in the late-21st century (2070-2099) can be explained by RCP 8.5 radiative forces increasing until 2100 causing more precipitation.

Comparing precipitation in the western sites (WR and WIC) to the eastern sites (ER, ER2, EIC, and EDC), under both RCPs 4.5 and 8.5, the western sites (WR and WIC) have statistically lower (p-value = <0.0001) precipitation than the eastern sites (ER, ER2, EIC, and EDC). The results of this statistical test confirm the visual west-east precipitation gradient among the sites (Figure 3).

Evapotranspiration Trends

ET was calculated as Hydrus-1D simulation outputs for each GCM, RCP, and site and ranged from 448 to 1,150 mm/yr (Figure 5). ET increased over time for each site and RCP, with more pronounced increases in RCP 8.5. Under both RCP 4.5 and 8.5, ET was statistically different in each time period (Steele-Dwass, p-value range = 0.0001-0.0018) which increased over time.

Under RCP 4.5, there were no statistical differences between each time period for all the eastern sites (ER, ER2, EIC, and EDC) (Steele-Dwass, p-value range = 0.3393-1.0). There were statistical differences between western (WR and WIC) and eastern sites (ER, ER2, EIC, and EDC) and between both western sites (WR and WIC) (p-values = <0.0001).

Under RCP 8.5, there were no statistical differences between each time period for the eastern sites (ER, ER2, EIC, and EDC) (p-value range = 0.3414-1.0). Under the late-21st century time period, both western sites (WR and WIC) had no statistical difference as well (Steele-Dwass, p-value = 0.2142). There were statistical differences between western (WR and WIC) and eastern sites (ER, ER2, EIC, and EDC) and between both western sites (WR and WIC) with the exception of the late-21st century (Steele-Dwass, p-values = <0.0001).

When comparing western to eastern sites, western sites have significantly higher ET (Figure 5). The simulated ET at western sites range from 788 to 1,150 mm/yr, while eastern sites range from 448 to 830 mm/yr.

Irrigation Requirement Trends

Irrigation requirements were calculated using Hydrus-1D outputs in CROPSIM as described earlier for sites WIC and EIC (Figure 6). There are no statistical differences in irrigation requirements between sites WIC and EIC under RCPs 4.5 and 8.5 during the first two time periods, historical (1950-2009) and early-21st century (2010-2039) (Steele-

Dwass, p-value range = 0.2693-0.9607). However, the two irrigation sites have statistical differences in irrigation requirements between RCPs 4.5 and 8.5 during the last two time periods, mid-21st century (2040-2069) and late-21st century (2070-2099), with larger irrigation requirements indicated in RCP 8.5 (Steele-Dwass, p-value range = <0.0001-0.0054). Under each RCP and time period, irrigation requirements for sites WIC and EIC were statistically different, with WIC requiring more irrigation than EIC (Steele-Dwass, p-value range = <0.0001-0.004). This reflects the precipitation gradient in the CPNRD where the western side of the study area has lower annual precipitation (Figure 3b).

Future Recharge Trends

The simulated recharge ranged from 0 to 715 mm/yr for the years 1950-2100 using the nine GCMs, RCPs of 4.5 and 8.5, and across all six study sites (Figure 7). Under both RCP 4.5 and 8.5 and at most of the six sites, the simulated median recharge was statistically lower (Steele-Dwass, p-value < 0.05) by the middle (2040-2069) to late (2070-2099) 20th century as compared to the historical period (1950-2009) (Figure 7). Because the temporal patterns of simulated recharge beneath each site, under each LULC type, and from east (higher annual precipitation) to west (lower annual precipitation) are generally very similar beneath both RCP 4.5 and 8.5 (Figure 7ab), the following presentation and discussion of results will focus on simulated recharge patterns under RCP 8.5.

Under RCP 8.5, each of the six sites had statistically different simulated median recharge rates during the historic period (Steele-Dwass, p-value = <0.0001), with the exception of sites WR and ER that had statistical similar historic recharge rates (Figure

7b). During the historical period, the greatest recharge rates were beneath the EIC, EDC, ER2, and WIC sites, respectively. The historical recharge rates beneath the WR and ER sites were nearly 100 mm/yr lower or more than the corresponding irrigated sites, as described below. Under the historical period, the simulated recharge beneath the western sites (WR and WIC) was statistically lower than beneath the eastern sites (ER, ER2, EIC, and EDC), based on results of the Kruskal-Wallis test (p -values = <0.0001). These east-west spatial patterns in simulated recharge rates are a response to substantially higher ET in the western sites compared to the eastern sites (Figure 5). The relatively lower precipitation and higher ET at the western sites limits the soil moisture below the root zone that eventually becomes recharge.

Under RCP 8.5, all six sites except for WIC and EIC have simulated recharge rates by the early-21st century (2010-2039) that are statistically lower than the corresponding historical period (Figure 7). By the middle (2040-2069) and for the late (2070-2099) 20th century, all six sites have statistically lower recharge than the historical period (p -value range = <0.0001 - 0.008) (Figure 7). These forecasted decreases in recharge rates are a response to the increased radiative forcings under RCP 8.5 that generally increase ET (Figure 5b) and irrigation requirements (Figure 6b) during the latter half of the 21st century.

Under RCP 8.5, all LULCs types (rangeland, irrigated corn, and dryland corn) for each time period have statistically different recharge rates (Steele-Dwass, p -value = <0.0001), with the exception of irrigated corn sites (WIC and EIC) and the dryland corn site (EDC) during the historic (1950-2009) and early-21st century (2010-2039) time periods

(Steele-Dwass, p-value range = 0.0959-0.9162). This indicates the sensitivity of corn crop sites under future climate change and the increased radiative forcings. Although both ER and ER2 sites are rangeland sites in the eastern part of the study area, site ER2 has statistically greater recharge than ER for all time periods (Figure 7b). The factors controlling these differences are explained using their respective total potential profiles in the following sections.

Historic Recharge Trends with Climate Variability

To further evaluate recharge response to climate extremes, I compared timeseries of the PDSI and the simulated recharge rates at the six sites over the historical period of 1950-2018 (Figure 8). Upon visual examination, the PDSI and recharge timeseries have similar timing of relatively high and low values at the western and eastern irrigated and dryland corn sites (WIC, EIC, and EDC) (Figures 8b, d, and f). These figures indicate that recharge beneath corn crops, regardless of irrigation, is relatively more responsive to wet and dry periods than the rangeland sites. Rangeland sites have very few, if any, similarities between the temporal variability phases of minimum and maximum PDSI and recharge timeseries and have opposing phases in some cases (Figures 8a, c, and e). Rangeland sites also showed pronounced seasonal dips in recharge compared to both irrigated and dryland corn crop sites. Although there appears to be some similarities between the PDSI and recharge timeseries at the irrigated sites, none of the six sites have statistically significant correlations (bivariate normal ellipse with a confidence of 0.95) between PDSI and recharge.

Given the time lag between any climate perturbation at land surface that affects ET and infiltration and the subsequent water flux down through the relatively thick vadose zone before recharging the water table, I also evaluated lag correlations between the PDSI and simulated historical recharge timeseries. Lag correlations between PDSI value and historical recharge timeseries were calculated using the software Hydroclimate with a 95% confidence level (Dickinson et al., 2014). A correlation coefficient was calculated for each site at lag times of 1-414 months (this is the number of months the historic recharge simulations were run). The lag time with the highest correlation coefficient for each site (Table 4) was then used to plot the phase-shifted simulated historic recharge timeseries against the PDSI value timeseries (Figure 9). Site WR is omitted from Figure 9 because no statistically significant lag correlation coefficients were detected within 30 years of phase lags, which is beyond the time of typical travels times of water flux through the vadose zone at this site. Visual examination of the phase-shifted recharge timeseries (Figure 9) indicate a much closer response to PDSI for most sites, especially in terms of peak values in recharge to the highest PDSI values. The simulated recharge at the corn crop sites have moderate lag correlation coefficients to PDSI with similar phase lag times of 20-24 months (Table 4). The recharge beneath the eastern rangeland sites (ER and ER2) has a much slower responses to PDSI with phase lag times of 108 and 58 months, respectively. These lag correlation results indicate that LULC is an important factor on recharge responses to climate variability.

Using the PDSI, ten historical wet and dry periods were chosen based on length and severity of the period (Table 5). In general, the median recharge per month for each site is relatively greater under wet periods (positive PDSI values) and lower under the dry periods (negative PDSI values) (Table 5). Comparison of recharge under all wet and dry conditions show statistical differences from wet and dry conditions for each site (Steele-Dwass, p-values = (ER) 0.0064 and (WR, WIC, ER2, EIC, EDC) <0.0001).

Historic Total Potential Profiles

Total potential profiles were simulated using the Hydrus-1D models for each of the six sites with recent historical atmospheric and meteorological inputs from the years 2008-2018 (Figure 10). The simulated head at vertical depths within the vadose zone for the first of every March, June, September, and December during the most recent dry and wet periods were used to calculate total potential profiles. The dates shown in Figure 10 were chosen because they encompass the most recent peak dry and wet PDSI values reported.

Most of the variability in the total potential profile occurs in the top few meters of the vadose zone, which is why Figure 10 depicts only the top few meters beneath each site. The deeper total potential profiles that are not shown in Figure 10 all generally have a downward and 1:1 unit gradient profile that indicates gravity dominated flow, which is similar to the total potential profiles shown in Figure 1a below approximately 3 m below land surface. Both western sites (WR and WIC) showed downward flux occurring shallower in the profile during the dry period compared to the wet period. The eastern sites (ER, ER2, EIC, and EDC) showed more downward flux in general, in the 2012 dry period

but with seasonal upward flux in the top meter for sites ER2, EIC, and EDC. This indicates that in times of drought, total potential in eastern sites, with greater average annual precipitation than the western sites, are more sensitive to seasonal fluctuation displaying periods of upward flux.

As mentioned earlier, the difference in the simulated recharge rates beneath ER and ER2 is explained by their contrasting total potential profiles (Figure 10ce). Site ER has a nearly vertical total potential slope, indicating little to no flux, except in the top 1/10thm of the vadose zone. The relatively lower total potential values are the result of relatively drier water contents and less water storage in the vadose zone. Whereas, site ER2 has much greater total potential values and wider fluctuations reaching deeper in the vadose zone and a more positive total potential slope, meaning large water content and relatively more downward flux compared to site ER.

The location, west versus east, seems to be a controlling factor on total potential profile responses to periods of drought and increased precipitation (Figure 10). The western sites (WR and WIC) total potential profiles respond as one would expect with less downward flux in periods of drought and more in periods of increased precipitation. The eastern sites receive more annual precipitation than the western sites but respond opposite to the western sites with less downward flux in periods of increased precipitation but the development of seasonal upward flux in times of drought.

Future Total Potential Profiles

Simulated future total potential profiles were constructed for each of the six sites using the CANESM2 GCM under RCP 4.5 (Figure 11) and RCP 8.5 (Figure 12). Hydrus-1D outputs of head at depth were used to calculate total potential profiles for the first of every March, June, September, and December for the years 2040 and 2099 and are displayed in Figures 11 and 12 to represent the change in radiative forcing at 2040 in RCP 4.5 compared to RCP 8.5 and its projected effect on future total potential responses. In both figures, only the top few meters of the vadose zone are depicted since each site displayed uniform total potential slopes below what is shown.

Under RCP 4.5 (Figure 11), not much variation in total potential profiles from 2040 to 2099 is displayed at any site. Strong seasonal variations can be seen in the corn crop sites (WIC, EIC, and EDC) with less wetting in the months of June and September compared to the months of December and March. The rangeland sites (WR, ER, and ER2) did not show as much seasonal variation. Instances of seasonal upward flux can be seen at each site with the exception of site ER.

Under RCP 8.5 (Figure 12), more variation is displayed in total potential profiles from 2040-2099 at each site, especially for the months of September and December, which seem to be the months with the lowest downward flux. Under RCP 8.5, each site displays seasonal upward flux in the year 2099.

Future projections of total potential profiles seem to be more directly controlled by LULC than location (west and east) as was the case with historic total potential

profiles. Seasonal variation is observed to be considerable at the corn crop sites under RCP 4.5 in 2099 but upward flux is seen at every site in 2099 under RCP 8.5. This indicates more seasonal upward flux, regardless of LULC, in the future if we experience climate change scenarios closer to that of RCP 8.5.

CONCLUSION

To understand how recharge may respond to climate variability and change in semi-arid to arid locations with thick vadose zones, I used Hydrus-1D to simulate historic and future recharge and total potential profiles of six study sites in the CPNRD of central Nebraska. I analyzed historic and future recharge and total potential profiles to assess controlling factors of recharge: land use/land cover (LULC), climate conditions (precipitation, air temperature), and recharge mechanisms (diffuse and irrigation recharge).

Historic precipitation data has shown a west/east gradient with higher precipitation in the east. Nine LOCA downscaled GCMs each at an RCP of 4.5 and 8.5 show projected increases in future precipitation for each of the six study sites with larger increases under RCP 8.5. The Penman-Monteith calculations from the GCMs inputs in Hydrus-1D indicate higher ET in the west than in the east and show projected increases in future ET for each of the six study sites with larger increases under RCP 8.5. CROPSIM calculated irrigation requirements for all the GCM Hydrus simulations for sites WIC and EIC indicate larger requirements in the west and are projected to increase over time at both sites under RCP 8.5.

Future projections of recharge simulated by the GCM input Hydrus-1D models indicate more recharge in the east than in the west with respect to LULC; this is consistent with the west/east precipitation gradient of the area. More recharge is projected under irrigated sites than their respective rangeland sites (west and east). Recharge is projected

to decrease at each site over time under RCP 8.5 climate change conditions. In the east, recharge under dryland corn, EDC, falls between ER and EIC. ER2 shows more recharge than ER but their total potential profiles shows that downward flux reaches deeper in the vadose zone under ER2 than ER, which has a nearly vertical total potential slope indicating very little flux in the vadose zone. These results indicate that climate conditions, particularly seen with the spatial and climate change GCM RCP 8.5 variations, and LULC are large controlling factors on recharge.

Historic recharge timeseries of each site, except WR, showed correlations to PDSI value timeseries after they were adjusted for phase lag times. Quicker responses in recharge to drought and high precipitation time periods indicated by PDSI values were seen in all three corn crop sites (WIC, EIC, and EDC) with lag times ranging from 20-24 months. All rangeland sites (WR, ER, and ER2) had much slower responses to drought and high precipitation time periods indicated by PDSI values with lag times ranging from 58-372 months. This indicates that LULC is the largest factor affecting climate variability recharge responses.

Historic total potential profiles of the most recent wet and dry period show western sites (WR and WIC), which receive lower annual average precipitation than eastern sites, to have less downward flux during dry periods compared to wet periods. The opposite is seen with the eastern sites (ER, ER2, EIC, and EDC); wet periods show less downward flux compared to dry periods. The eastern sites, however, show seasonal upward flux during the dry period. This indicates that all sites' total potential profiles respond to wet

and dry periods, but differ in their responses based on their location, or rather their annual average precipitation because of the east/west precipitation gradient seen in the study site.

Future total potential profiles for the years 2040 and 2099 show similar total potential profile patterns to that of the historic. Seasonal variation is considerable at the corn crop sites under RCP 4.5 in 2099 but upward flux is seen at every site in 2099 under RCP 8.5. This indicates more seasonal upward flux, regardless of LULC, in the future if we experience climate change scenarios closer to that of RCP 8.5

These findings give a better understanding of the factors that affect recharge rates and mechanisms in thick vadose zones of semi-arid and arid climates and can hopefully be used to improve the inflow component of future groundwater budgets and inform groundwater sustainability planning and related policy decisions.

TABLES

Table 1. Vadose zone monitoring well sites in the CPNRD used in this study adapted from Lauffenburger et al., 2018; note: the depth to water values were recorded at the time of well installation between 2008-2013.

Site	USGS Site ID	Depth to water (bls, m)	Land surface elevation (m)	Latitude	Longitude
western rangeland (WR)	405738099504501	14.2	778	40°57'38.3"	-099°50'44.8"
western irrigated corn (WIC)	405855100073901	17.7	803	40°58'54.7"	-100°07'38.8"
eastern rangeland (ER)	410102098374201	20.2	607	41°01'02.5"	-098°37'41.7"
eastern rangeland 2 (ER2)	405435098432601	20.6	625	40°54'34.9"	-098°43'26.4"
eastern irrigated corn (EIC)	405855098383001	27.7	618	40°58'55.4"	-098°38'30.1"
eastern dryland corn (EDC)	405503098441801	38.9	647	40°55'02.7"	-098°44'18.2"

[Note: bls, below land surface; m, meters; Land surface elevation above sea level using the North American Vertical Datum of 1988; latitude and longitude North American Datum of 1983; USGS site data available in the USGS National Water Information System (NWIS), <http://waterdata.usgs.gov/nwis>].

Table 2. Nash-Sutcliffe coefficient of efficiency (NSE) values of observed versus simulated monthly total potential profile slopes for calibration.

Site	Dates	NSE Value
WR	4/2010-7/2017	-1.33
WIC	4/2010-4/2011	-2.76
ER	10/2011-11/2017	-0.71
ER2	12/2014-11/2017	-0.39
EIC	10/2008-12/2015	0.81
EDC	12/2014-11/2017	-0.03

Table 3: Output from these global climate models (GCMs) was downscaled and used in this study.

Abbreviation	Organization
CANESM2	Canadian Centre for Climate Modelling and Analysis
CNRM-CM5	Centre National de Recherches Météorologiques / Centre Européen de Recherche et Formation Avancée en Calcul Scientifique
CSIRO-MK3-6-0	Commonwealth Scientific and Industrial Research Organization in collaboration with Queensland Climate Change Centre of Excellence
GFDL-ESM2G	NOAA Geophysical Fluid Dynamics Laboratory
INMCM4	Institute for Numerical Mathematics
MIROC5	Atmosphere and Ocean Research Institute (The University of Tokyo), National Institute for Environmental Studies, and Japan Agency for Marine- Earth Science and Technology
MPI-ESM-LR	Max-Planck-Institut für Meteorologie (Max Planck Institute for Meteorology)
MRI-CGCM3	Meteorological Research Institute
NORES1-M	Norwegian Climate Centre

Table 4. Lag correlations of simulated historic recharge timeseries calculated in Hydrus-1D and PDSI value timeseries.

PDSI Lag Correlations		
Site	Phase lag (months)	Correlation Coefficients
WIC	24	0.413
ER	108	0.342
ER2	58	0.543
EIC	22	0.566
EDC	20	0.567

Table 5. Historic wet and dry periods chosen for comparison based on PDSI values with modeled historic median recharge of each period.

	Time Period [month/year]	Duration [months]	PDSI min.	PDSI max.	PDSI median	Median Recharge [mm/month]					
						WR	WIC	ER2	ER	EIC	EDC
Wet Periods	1/1950-5/1952	29	0.67	7.13	3.10	0.15	6.03	14.3	2.28	20.0	14.4
	5/1982-1/1988	69	1.15	6.19	3.34	0.22	9.97	17.9	1.99	30.7	12.6
	7/1992-8/1999	86	0.89	8.23	3.44	0.23	13.0	15.9	2.97	28.0	14.1
	12/2006-8/2011	57	1.28	7.40	4.64	0.29	19.1	20.7	2.54	29.8	8.93
	6/2014-12/2018	51	0.57	5.36	2.31	0.33	8.85	9.20	1.98	19.3	16.3
Dry Periods	8/1953-3/1957	44	-7.11	-1.06	-4.20	0.15	5.74	8.90	2.23	17.1	16.2
	7/1974-2/1977	32	-3.17	-0.67	-1.62	0.21	7.84	13.0	1.48	25.4	11.1
	6/1988-9/1991	40	-4.50	-0.71	-3.20	0.23	16.7	10.6	2.43	21.0	19.1
	3/2002-8/2004	30	-4.87	-1.17	-3.05	0.24	8.75	8.31	3.02	16.7	16.9
	3/2012-5/2014	27	-6.34	-1.10	-3.29	0.31	11.3	14.9	2.00	26.6	22.0

FIGURES

Figure 1. (a) Seasonal fluctuations in total potential in northern High Plains rangeland. (b) Persistent upward flux in arid southern High Plains rangeland. Data is modified from (a) Steele et al., 2014 (b) Gurdak et al., 2007.

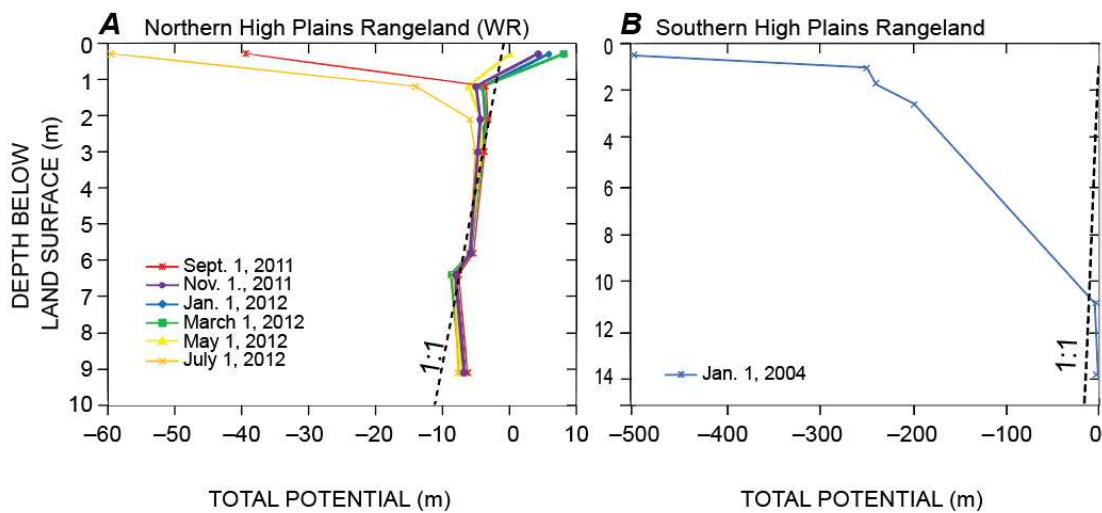


Figure 2. Central Platte Natural Resources District (CPNRD) land use map. Sites used in this study: 1, 2, 3, 4, 6, and 8, abbreviated at ER, EIC, EDC, ER2, WIC, and WR respectively. Image credit to Steele et al., 2014.

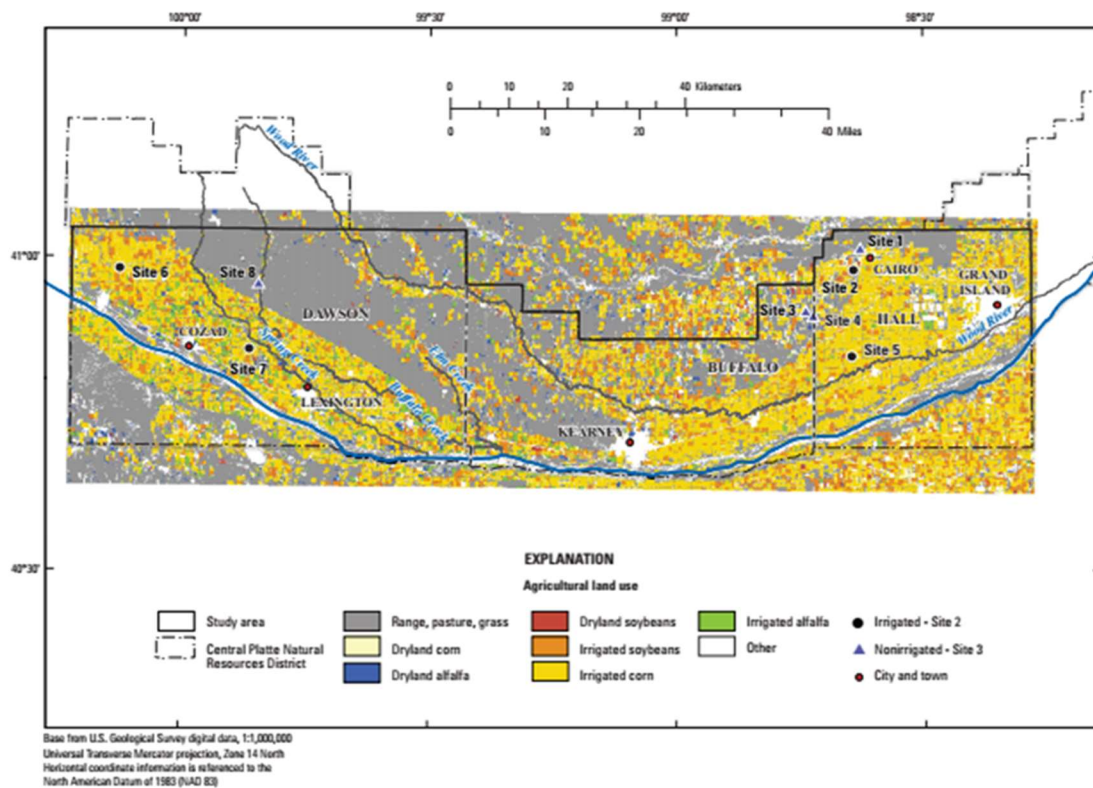


Figure 3. Location of the northern High Plains rangeland and agricultural study sites on the distribution of regional (a) mean annual air temperature and (b) mean annual precipitation (modified from Lauffenburger et al., 2018 and McMahon et al., 2007). The study includes the western rangeland (WR), western irrigated corn (WIC), eastern rangelands (ER and ER2), eastern irrigated corn (EIC), and eastern dryland corn (EDC) sites in the Central Platte Natural Resources District (CPNRD). Air temperature and precipitation data credit to Thornton et al., (1997).

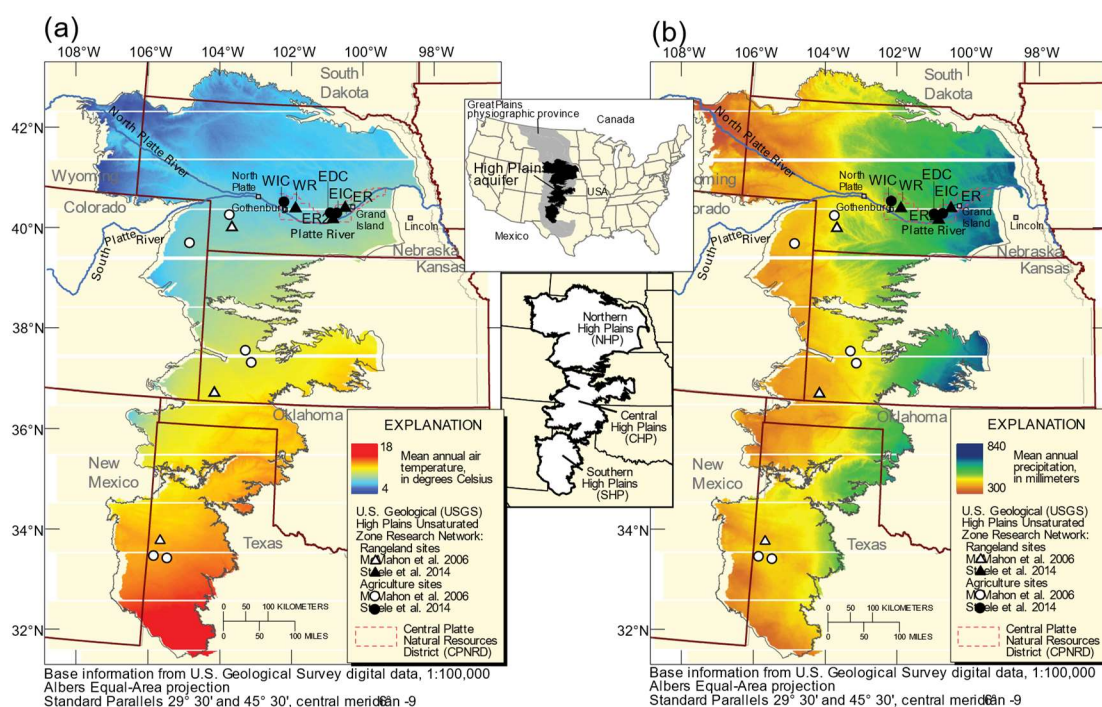


Figure 4. Simulated historic (1950-2009) and future (2010-2100) precipitation (mm/yr) at each of the six study sites (western rangeland (WR), western irrigated corn (WIC), eastern rangeland (ER), eastern rangeland 2 (ER2), eastern irrigated corn (EIC), and eastern dryland corn (EDC)) based on LOCA downscaled output from nine GCMs using (a) RCP 4.5 and (b) RCP 8.5.

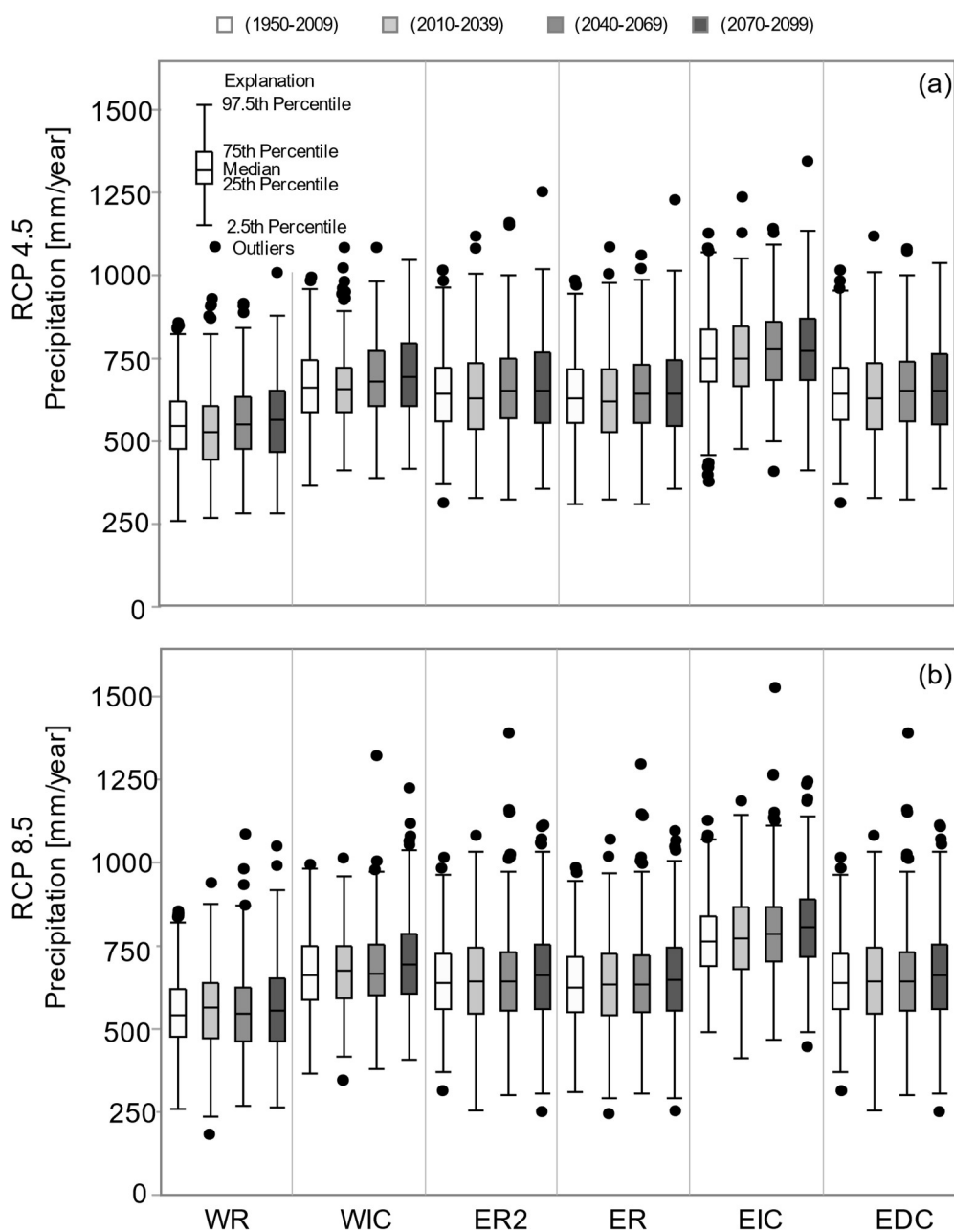


Figure 5. Simulated historic (1950-2009) and future (2010-2100) evapotranspiration (ET) (mm/yr) from Hydrus-1D at each of the six study sites (western rangeland (WR), western irrigated corn (WIC), eastern rangeland (ER), eastern rangeland 2 (ER2), eastern irrigated corn (EIC), and eastern dryland corn (EDC)) based on LOCA downscaled output from nine GCMs using (a) RCP 4.5 and (b) RCP 8.5.

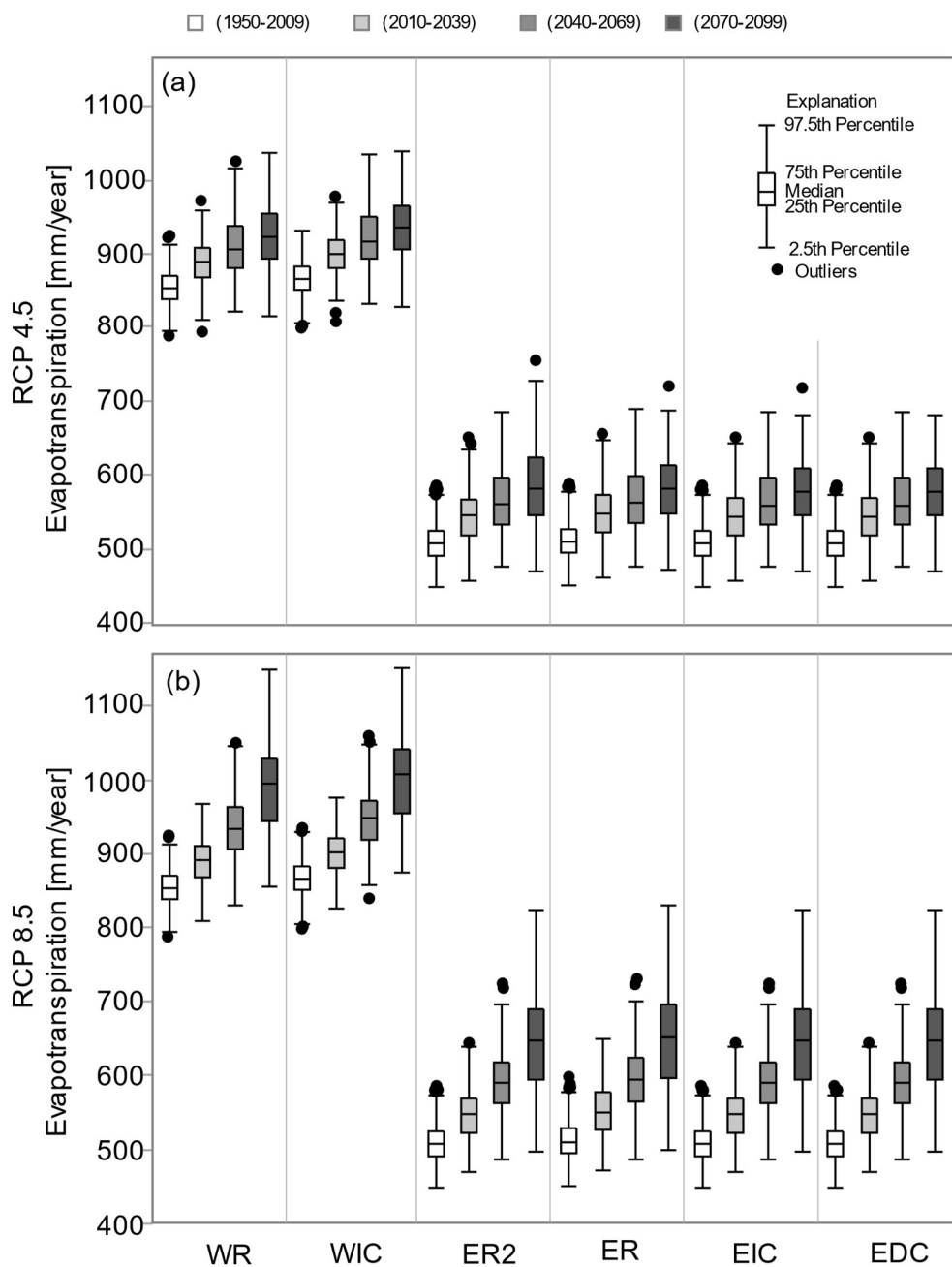


Figure 6. Simulated historic (1950-2009) and future (2010-2100) irrigation requirements (mm/yr) from Hydrus-1D at each both irrigated corn sites (western irrigated corn (WIC), eastern irrigated corn (EIC)) based on LOCA downscaled output from nine GCMs using (a) RCP 4.5 and (b) RCP 8.5.

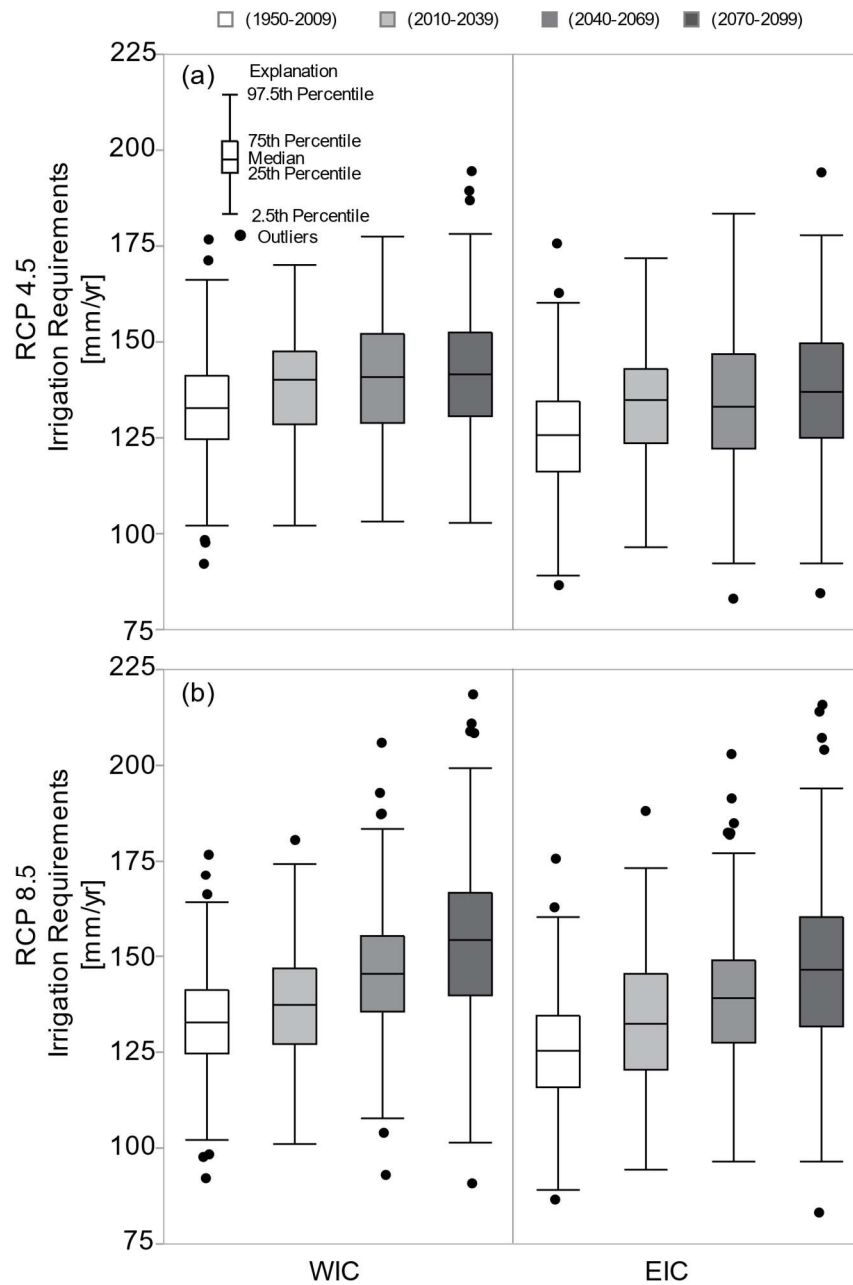


Figure 7. Simulated historic (1950-2009) and future (2010-2100) recharge (mm/yr) from Hydrus-1D at each of the six study sites (western rangeland (WR), western irrigated corn (WIC), eastern rangeland (ER), eastern rangeland 2 (ER2), eastern irrigated corn (EIC), and eastern dryland corn (EDC)) based on LOCA downscaled output from nine GCMs using (a) RCP 4.5 and (b) RCP 8.5.

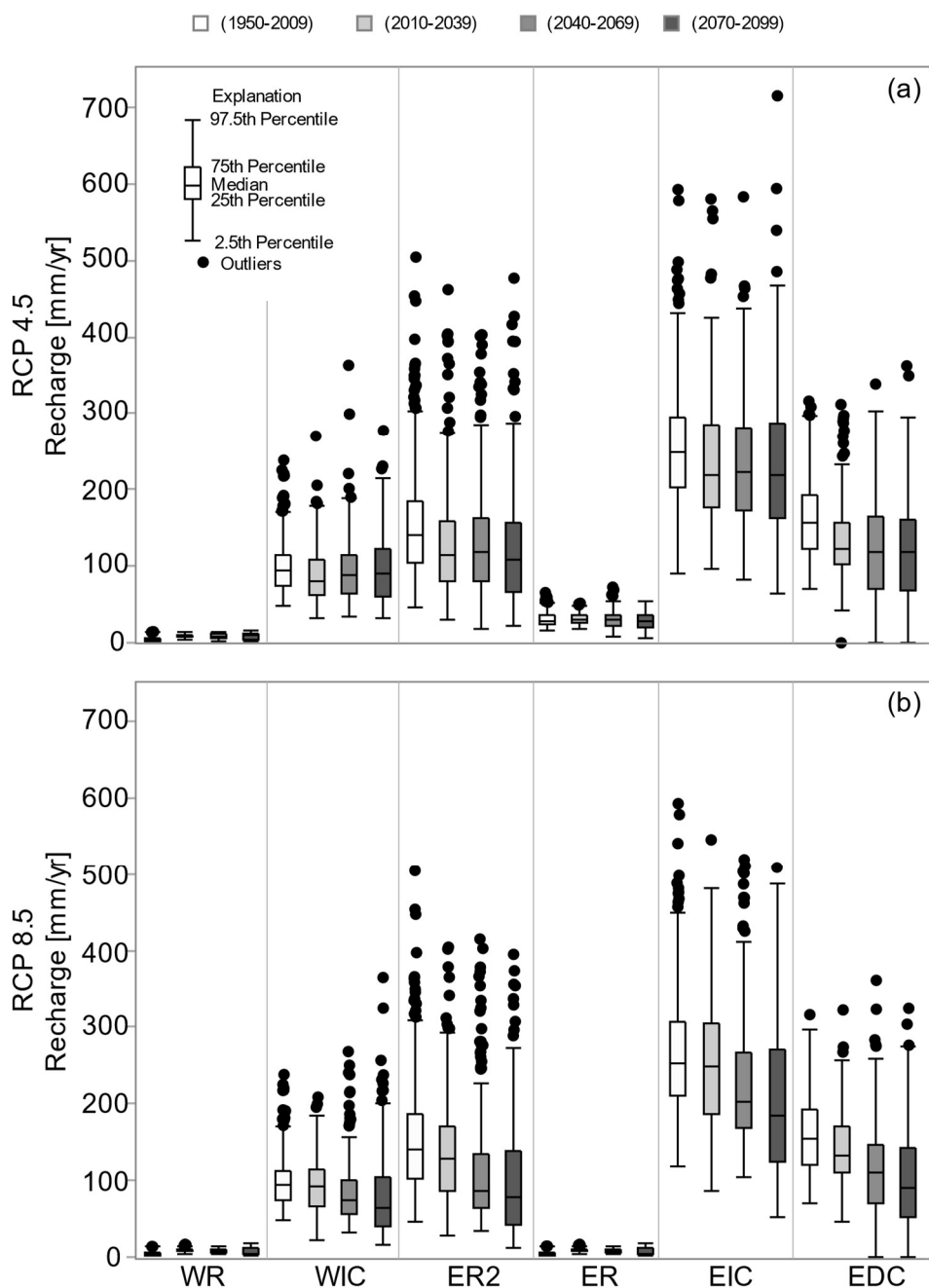


Figure 8. Simulated historic recharge (mm/month) from Hydrus-1D (left y-axis) with PDSI values (right y-axis) to show peak wet and dry periods over the period 1950-2018 for sites (a) western rangeland (WR), (b) western irrigated corn (WIC), (c) eastern rangeland (ER), (d) eastern irrigated corn (EIC), (e) eastern rangeland 2 (ER2), and (f) eastern dryland corn (EDC).

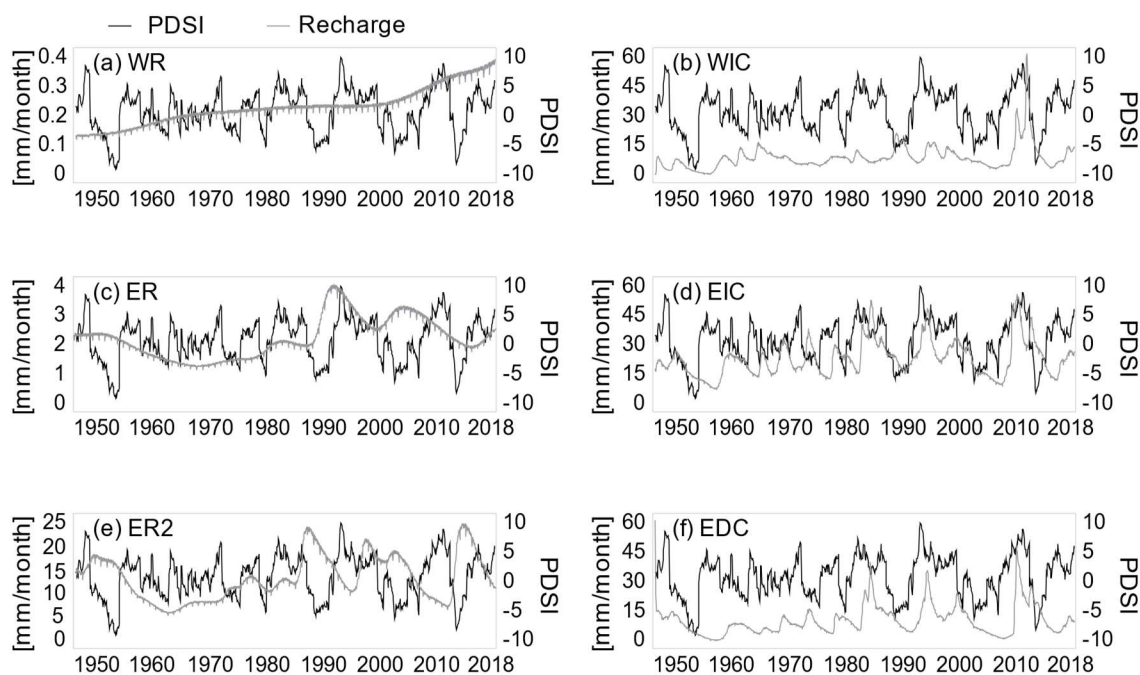


Figure 9. Simulated historic recharge (mm/month) from Hydrus-1D (left y-axis) with PDSI values (right y-axis) adjusted with lag correlations over the period 1950-2018 for sites, (a) western irrigated corn (WIC) with a lag time of 24 months, (b) eastern rangeland (ER) with a lag time of 108 months, (c) eastern irrigated corn (EIC) with a lag time of 22 months, (d) eastern rangeland 2 (ER2) with a lag time of 58 months, and (e) eastern dryland corn (EDC) with a lag time of 20 months.

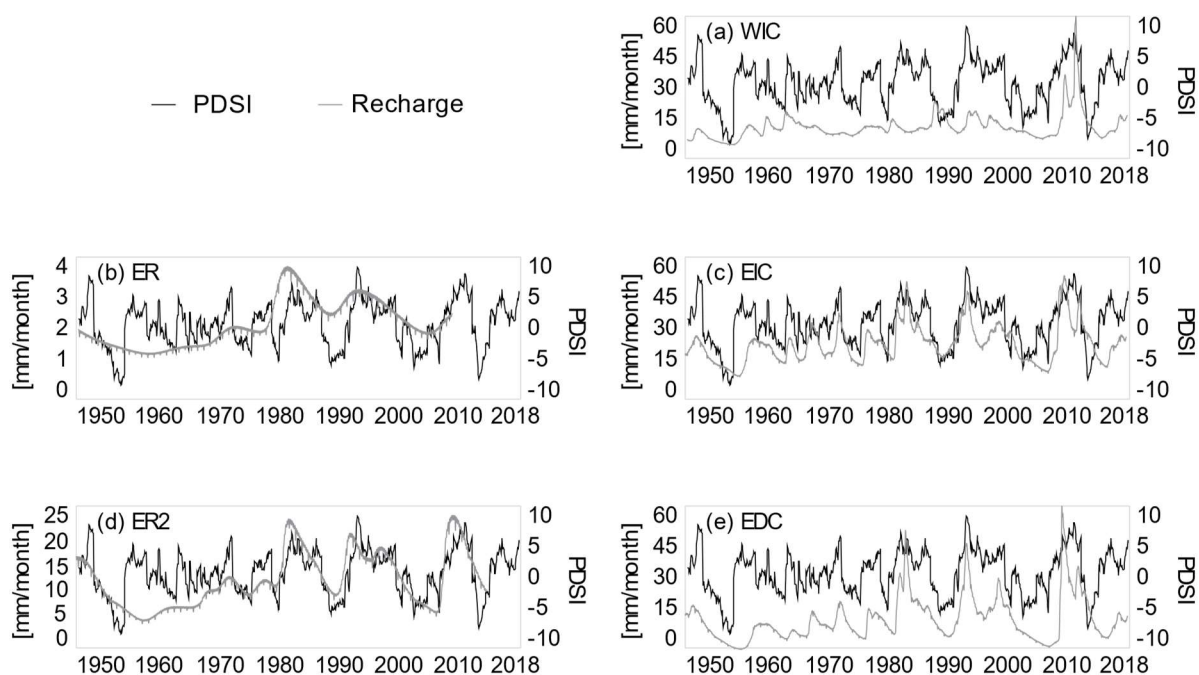


Figure 10. Recent historical total potential profiles of calculated from Hydrus-1D head at depth output at sites (a) western rangeland (WR), (b) western irrigated corn (WIC), (c) eastern rangeland (ER), (d) eastern irrigated corn (EIC), (e) eastern rangeland 2 (ER2), and (f) eastern dryland corn (EDC). The dashed lines represent profiles centered on the most recent dry period in Central Nebraska and solid lines represent profiles centered on the most recent wet period in Central Nebraska. Only the top few meters are shown to clearly depict the variability there.

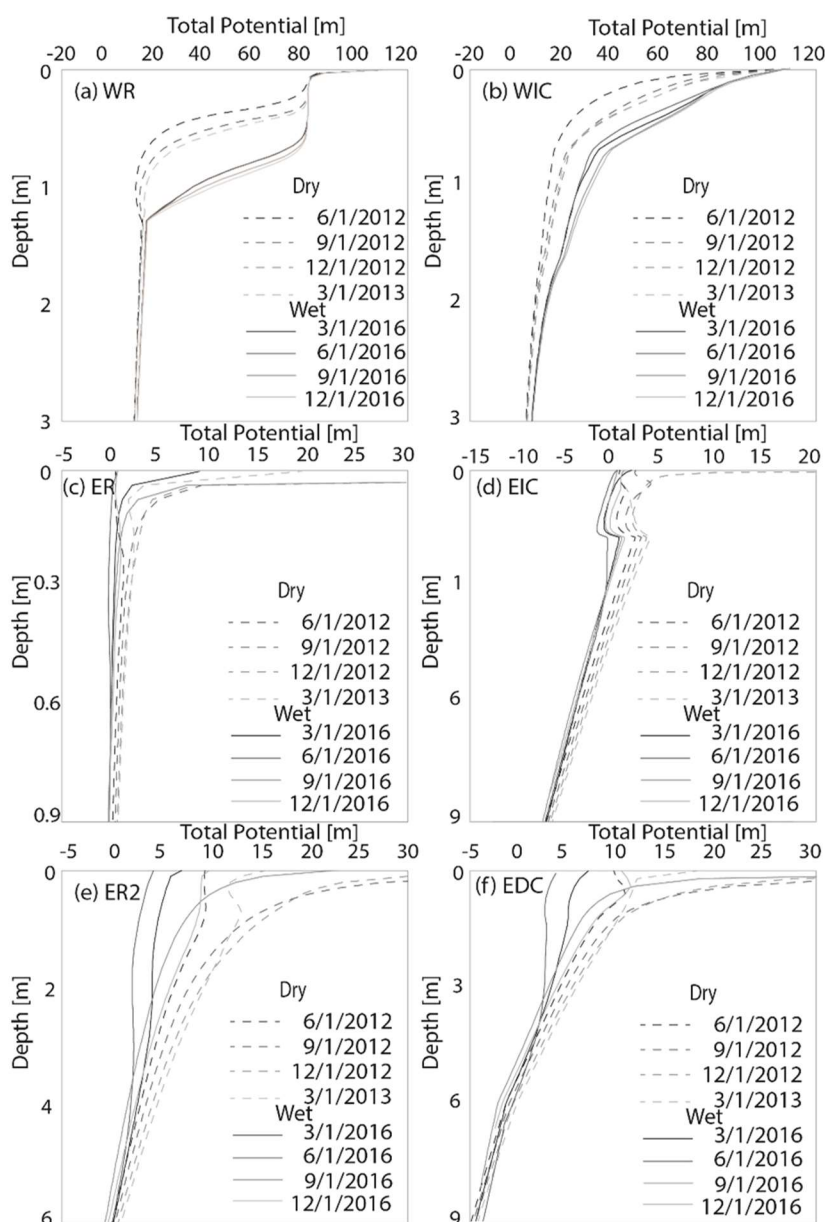


Figure 11. Simulated future total potential profiles of GCMs at RCP 4.5 calculated from Hydrus-1D head at depth output at sites (a) western rangeland (WR), (b) western irrigated corn (WIC), (c) eastern rangeland (ER), (d) eastern irrigated corn (EIC), (e) eastern rangeland 2 (ER2), and (f) eastern dryland corn (EDC). Dashed lines represent months in the year 2040 and solid lines represent months in the year 2099.

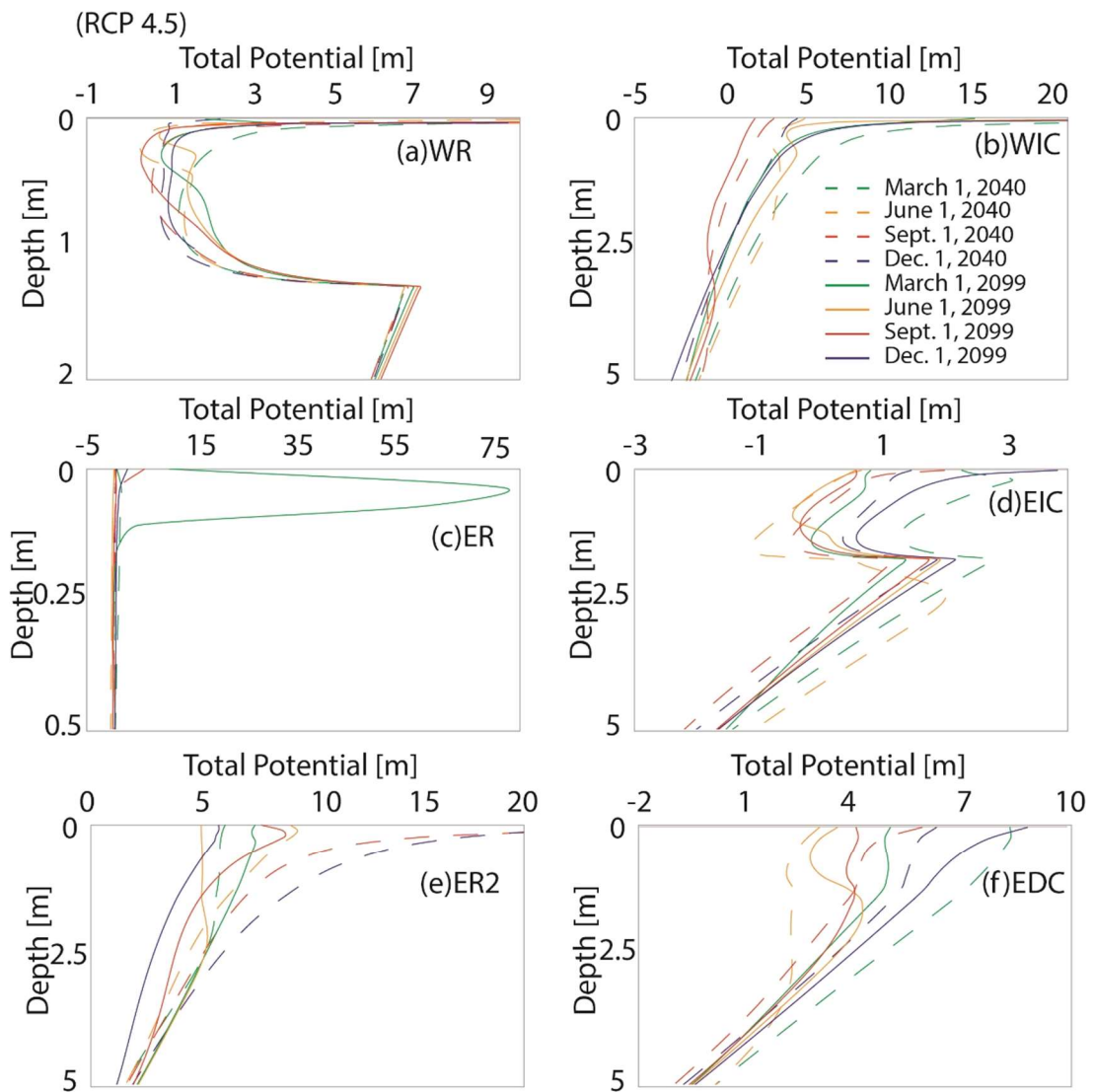
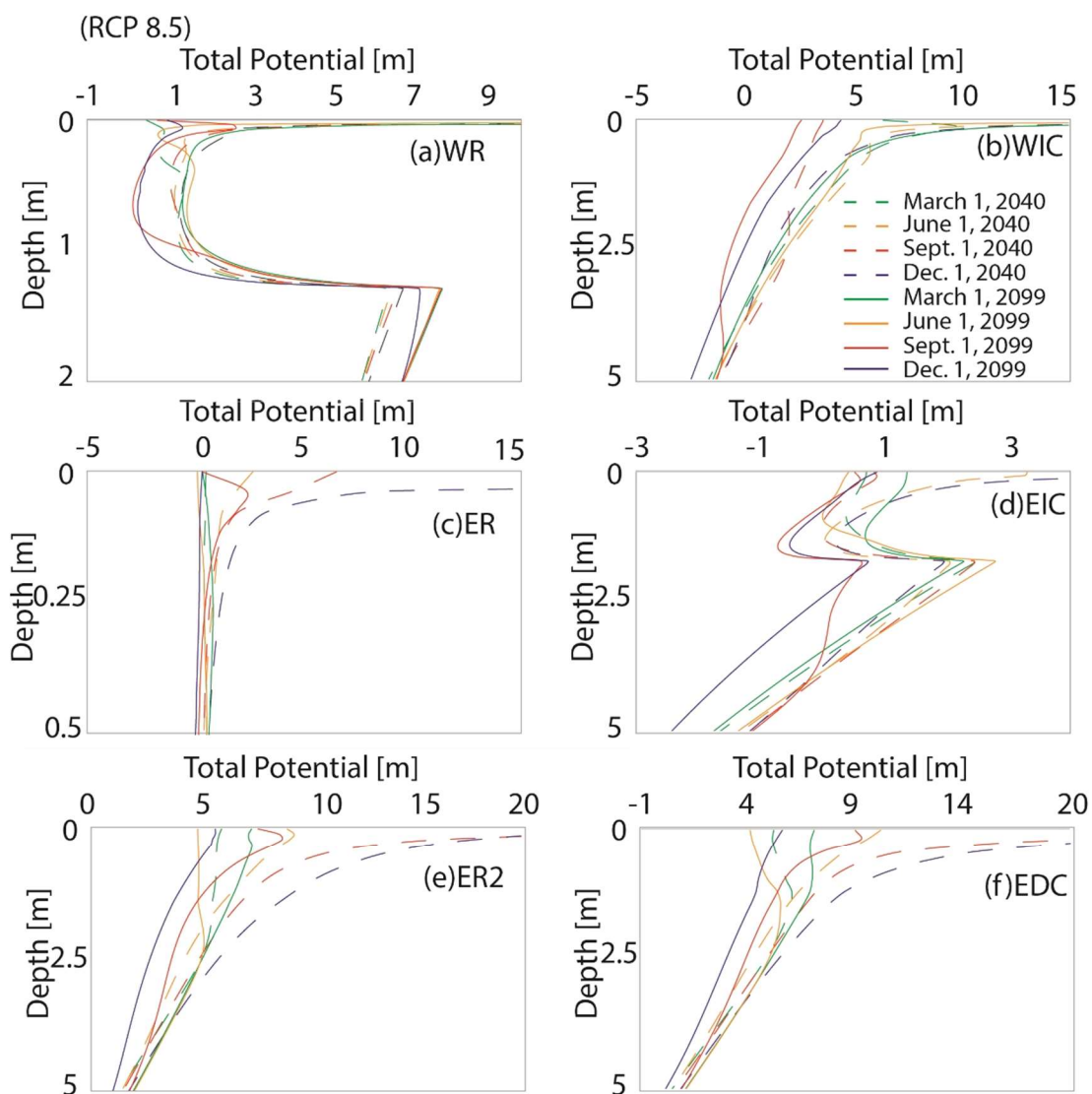


Figure 12. Simulated future total potential profiles of GCMs at RCP 8.5 calculated from Hydrus-1D head at depth output at sites (a) western rangeland (WR), (b) western irrigated corn (WIC), (c) eastern rangeland (ER), (d) eastern irrigated corn (EIC), (e) eastern rangeland 2 (ER2), and (f) eastern dryland corn (EDC). Dashed lines represent months in the year 2040 and solid lines represent months in the year 2099.



REFERENCES

- Ajami, H., McCabe, M.F., Evans, J.P., Stisen, S., 2014. Assessing the impact of model spin-up on surface water-groundwater interactions using an integrated hydrologic model. *Water Resour. Res.* 50, 2636–2656.
<https://doi.org/10.1002/2013WR014258>
- Anderson, M.P., Woessner, W.W., Hunt, R.J., 2015. *Applied Groundwater Modeling: Simulation of Flow and Advective Transport*, Second. ed. Academic Press.
- Bracken, C., 2016. Downscaled CMIP3 and CMIP5 Climate Projections-Addendum, Release of Downscaled CMIP5 Climate Projections (LOCA) and Comparison with Preceding Information. US Dep. Inter. Bur. Reclam.
- Campbell Scientific Inc., 2009. 229 Heat Dissipation Matric Water Potential Sensor Instruction Manual.
- Clarke, L., Edmonds, J., Pitcher, H., Reilly, J., Richels, R., 2007. Scenarios of Greenhouse Gas Emissions and Atmospheric Concentrations.
- Crosbie, R.S., Scanlon, B.R., Mpelasoka, F.S., Reedy, R.C., Gates, J.B., Zhang, L., 2013. Potential climate change effects on groundwater recharge in the High Plains Aquifer, USA: Climate Change Effects on Recharge in the High Plains. *Water Resour. Res.* 49, 3936–3951. <https://doi.org/10.1002/wrcr.20292>
- Dickinson, J.E., Hanson, R.T., Predmore, S.K., 2014. HydroClimATe—Hydrologic and Climatic Analysis Toolkit, in: *Hydrologic Analysis and Interpretation, Techniques and Methods*. U.S. Geological Survey, Reston, Virginia, p. 48.
- Feddes, R.A., Kowalik, P.J., Zaradny, H., 1978. *Simulation of field water use and crop yield, Simulation monographs*. Wiley, New York.
- Green, T.R., Taniguchi, M., Kooi, H., Gurdak, J.J., Allen, D.M., Hiscock, K.M., Treidel, H., Aureli, A., 2011. Beneath the surface of global change: Impacts of climate change on groundwater. *J. Hydrol.* 405, 532–560.
<https://doi.org/10.1016/j.jhydrol.2011.05.002>
- Gurdak, J.J., Hanson, R.T., McMahan, P.B., Bruce, B.W., McCray, J.E., Thyne, G.D., Reedy, R.C., 2007. Climate variability controls on unsaturated water and chemical movement, High Plains aquifer, USA. *Vadose Zone J.* 6, 533.
<https://doi.org/10.2136/vzj2006.0087>
- Gurdak, J.J., McMahan, P.B., Dennehy, K.F., Qi, S.L., 2009. Water Quality in the High Plains aquifer, Colorado, Kansas, Nebraska, New Mexico, Oklahoma, South Dakota, Texas, and Wyoming, 1999-2004. *Geol. Surv. Circ.* 63.
- Helsel, D.R., Hirsch, R.M., 1992. *Statistical methods in water resources*. Elsevier.
- Konikow, L.F., 2015. Long-Term Groundwater Depletion in the United States. *Groundwater* 53, 2–9. <https://doi.org/10.1111/gwat.12306>
- Konikow, L.F., 2013. *Groundwater depletion in the United States (1900-2008)*. US Department of the Interior, US Geological Survey, Reston, Virginia.
- Kuss, A.J.M., Gurdak, J.J., 2014. Groundwater level response in U.S. principal aquifers to ENSO, NAO, PDO, and AMO. *J. Hydrol.* 519, 1939–1952.
<https://doi.org/10.1016/j.jhydrol.2014.09.069>

- Lauffenburger, Z.H., Gurdak, J.J., Hobza, C., Woodward, D., Wolf, C., 2018. Irrigated agriculture and future climate change effects on groundwater recharge, northern High Plains aquifer, USA. *Agric. Water Manag.* 204, 69–80.
<https://doi.org/10.1016/j.agwat.2018.03.022>
- Li, H., Sheffield, J., Wood, E.F., 2010. Bias correction of monthly precipitation and temperature fields from Intergovernmental Panel on Climate Change AR4 models using equidistant quantile matching. *J. Geophys. Res.* 115, D10101.
<https://doi.org/10.1029/2009JD012882>
- McMahon, P.B., Dennehy, K.F., Bruce, B.W., Böhlke, J.K., Michel, R.L., Gurdak, J.J., Hurlbut, D.B., 2006. Storage and transit time of chemicals in thick unsaturated zones under rangeland and irrigated cropland, High Plains, United States. *Water Resour. Res.* 42, n/a-n/a. <https://doi.org/10.1029/2005WR004417>
- McMahon, P.B., Dennehy, K.F., Bruce, B.W., Gurdak, J.J., Qi, S.L., 2007. Water-Quality Assessment of the High Plains Aquifer, 1999-2004. *US Geol. Surv.* 136.
- McMahon, P.B., Dennehy, K.F., Michel, R.L., Sophocleous, M.A., Ellett, K.M., Hurlbut, D.B., 2003. Water movement through thick unsaturated zones overlying the central High Plains aquifer, southwestern Kansas, 2000-2001 39.
- McMahon, P.B., Plummer, L.N., Böhlke, J.K., Shapiro, S.D., Hinkle, S.R., 2011. A comparison of recharge rates in aquifers of the United States based on groundwater-age data. *Hydrogeol. J.* 19, 779–800.
- Meixner, T., Manning, A.H., Stonestrom, D.A., Allen, D.M., Ajami, H., Blasch, K.W., Brookfield, A.E., Castro, C.L., Clark, J.F., Gochis, D.J., Flint, A.L., Neff, K.L., Niraula, R., Rodell, M., Scanlon, B.R., Singha, K., Walvoord, M.A., 2016. Implications of projected climate change for groundwater recharge in the western United States. *J. Hydrol.* 534, 124–138.
<https://doi.org/10.1016/j.jhydrol.2015.12.027>
- NOAA, 2018. National Climatic Data Center.
- Pierce, D.W., Cayan, D.R., Maurer, E.P., Abatzoglou, J.T., Hegewisch, K.C., 2015. Improved Bias Correction Techniques for Hydrological Simulations of Climate Change. *J. Hydrometeorol.* 16, 2421–2442. <https://doi.org/10.1175/JHM-D-14-0236.1>
- Pierce, D.W., Cayan, D.R., Thrasher, B.L., 2014. Statistical Downscaling Using Localized Constructed Analogs (LOCA). *J. Hydrometeorol.* 15, 2558–2585.
<https://doi.org/10.1175/JHM-D-14-0082.1>
- Polade, S.D., Gershunov, A., Cayan, D.R., Dettinger, M.D., Pierce, D.W., 2013. Natural climate variability and teleconnections to precipitation over the Pacific-North American region in CMIP3 and CMIP5 models: CLIMATE VARIABILITY IN CMIP5 MODELS. *Geophys. Res. Lett.* 40, 2296–2301.
<https://doi.org/10.1002/grl.50491>
- Radcliffe, D.E., J.S., J., 2010. *Soil Physics with HYDRUS: modeling and applications.* CRC press.
- RCP Database (version 2.0), 2009.

- Riahi, K., Grueble, A., Nakicenovic, N., 2007. Scenarios of long-term socio-economic and environmental development under climate stabilization. *Technol. Forecast. Soc. Change* 74, 887–935.
- Richards, L., 1931. Capillary conduction of liquids in porous mediums. *Physics* 1, 318–333.
- Scanlon, B.R., Keese, K., Reedy, R.C., Simunek, J., Andraski, B.J., 2003. Variations in flow and transport in thick desert vadose zones in response to paleoclimatic forcing (0-90 kyr): Field measurements, modeling, and uncertainties: FLOW IN VADOSE ZONES IN RESPONSE TO PALEOCLIMATIC FORCING. *Water Resour. Res.* 39. <https://doi.org/10.1029/2002WR001604>
- Scanlon, B.R., Reedy, R.C., Stonestrom, D.A., Prudic, D.E., Dennehy, K.F., 2005. Impact of land use and land cover change on groundwater recharge and quality in the southwestern US. *Glob. Change Biol.* 11, 1577–1593. <https://doi.org/10.1111/j.1365-2486.2005.01026.x>
- Schaap, M.G., Leij, F.J., van Genuchten, M.T., 2001. ROSETTA: a computer program for estimating soil hydraulic parameters with hierarchical pedotransfer functions. *J. Hydrol.* 251, 163–176.
- Seck, A., Welty, C., Maxwell, R.M., 2015. Spin-up behavior and effects of initial conditions for an integrated hydrologic model: Spin-up behavior and effects of initial conditions. *Water Resour. Res.* 51, 2188–2210. <https://doi.org/10.1002/2014WR016371>
- Šimunek, J., Sejna, M., Saito, H., Sakai, M., van Genuchten, M.T., 2013. The HYDRUS-1D Software Package for Simulating the One-Dimensional Movement of Water, Heat, and Multiple Solutes in Variably-Saturated Media. Department of Environmental Sciences University of California Riverside.
- Šimunek, J., van Genuchten, M.Th., Šejna, M., 2008. Development and Applications of the HYDRUS and STANMOD Software Packages and Related Codes. *Vadose Zone J.* 7, 587–600. <https://doi.org/10.2136/vzj2007.0077>
- Smith, S.J., Wigley, T.M.L., 2006. Multi-Gas Forcing Stabilization with Minicam. *Energy J.* SI2006. <https://doi.org/10.5547/ISSN0195-6574-EJ-VolSI2006-NoSI3-19>
- Steele, G.V., Gurdak, J.J., Hobza, C.M., 2014. Water Movement through the Unsaturated Zone of the High Plains Aquifer in the Central Platte Natural Resources District, Nebraska, 2008–12.
- Stocker, T. (Ed.), 2014. *Climate change 2013: the physical science basis: Working Group I contribution to the Fifth assessment report of the Intergovernmental Panel on Climate Change.* Cambridge University Press, New York.
- Taylor, K.E., Stouffer, R.J., Meehl, G.A., 2012. An Overview of CMIP5 and the Experiment Design. *Bull. Am. Meteorol. Soc.* 93, 485–498. <https://doi.org/10.1175/BAMS-D-11-00094.1>
- Taylor, R.G., Scanlon, B., Döll, P., Rodell, M., van Beek, R., Wada, Y., Longuevergne, L., Leblanc, M., Famiglietti, J.S., Edmunds, M., Konikow, L., Green, T.R., Chen,

- J., Taniguchi, M., Bierkens, M.F.P., MacDonald, A., Fan, Y., Maxwell, R.M., Yechieli, Y., Gurdak, J.J., Allen, D.M., Shamsudduha, M., Hiscock, K., Yeh, P.J.-F., Holman, I., Treidel, H., 2012. Ground water and climate change. *Nat. Clim. Change* 3, 322–329. <https://doi.org/10.1038/nclimate1744>
- Thornton, P.E., Running, S.W., White, M.A., 1997. Generating surfaces of daily meteorological variables over large regions of complex terrain. *J. Hydrol.* 190, 214–251. [https://doi.org/10.1016/S0022-1694\(96\)03128-9](https://doi.org/10.1016/S0022-1694(96)03128-9)
- Treidel, H., Martin-Bordes, J.L., Gurdak, J.J. (Eds.), 2012. *Climate change effects on groundwater resources: a global synthesis of findings and recommendations*, 1st ed. ed. CRC Press/Balkema, Leiden, Netherlands ; Boca Raton [Fla.].
- Walvoord, M.A., Stonestrom, D.A., Andraski, B.J., Striegl, R.G., 2004. Constraining the Inferred Paleohydrologic Evolution of a Deep Unsaturated Zone in the Amargosa Desert. *Vadose Zone J.* 3, 502–512. <https://doi.org/10.2136/vzj2004.0502>
- Wellings, S.R., Bell, J.P., 1982. Physical controls of water movement in the unsaturated zone. *Q J Eng Geol Lond.* 15, 235–241.
- Wesseling, J.G., Elbers, J.A., Kabat, P., Van den Broek, B.J., 1991. SWATRE: Instructions for input.
- Wise, M., Calvin, K., Thomson, A., Clarke, L., Bond-Lamberty, B., Sands, R., Smith, S., Janetos, A., Edmonds, J., 2009. Implications of Limiting CO₂ Concentrations for Land Use and Energy. *Science* 1183–1186.